Pathophysiological function of endogenous calcitonin gene-related peptide in ocular vascular diseases

Yuichi Toriyama[1,2], Yasuhiro Iesato[1,2], Akira Imai[1,2], Takayuki Sakurai[1], Akiko Kamiyoshi[1], Yuka Ichikawa-Shindo[1], Hisaka Kawate[1], Akihiro Yamauchi[1], Kyoko Igarashi[1], Megumu Tanaka[1], Tian Liu[1], Xian Xian[1], Liuyu Zhai[1], Shinji Owa[1], Toshinori Murata[2], Takayuki Shindo[1]

[1] Department of Cardiovascular Research, Shinshu University Graduate School of Medicine, Japan

[2] Department of Ophthalmology, Shinshu University School of Medicine, Japan

Short running head: CGRP in the ocular vascular diseases

Number of text pages 35
Number of tables 2
Number of figures 12

Address for correspondence

Takayuki Shindo, MD, PhD

Department of Cardiovascular Disease,

Shinshu University Graduate School of Medicine

Asahi 3-1-1, Matsumoto, Nagano, 390-8621, Japan

Tel: +81-263-37-2578

Fax: +81-263-37-3437

Email: tshindo@shinshu-u.ac.jp

Abbreviations

CGRP; calcitonin gene-related peptide

AM; adrenomedullin

CLR; calcitonin receptor-like receptor

RAMP; receptor activity-modifying protein

WT; wild-type

OIR; oxygen-induced retinopathy

CNV; choroid neovascularization

AMD; age-related macular degeneration

RPE; retinal pigment epithelium

FA; Fluorescent angiography

Abstract

Calcitonin gene-related peptide (CGRP) has a variety of functions and exhibits both angiogenic and anti-inflammatory properties. We previously reported the angiogenic effects of adrenomedullin (AM), another CGRP family peptide, in oxygen-induced retinopathy (OIR); however, the effects of CGRP on ocular angiogenesis remain unknown. In the present study, we used CGRP knockout (CGRP-/-) mice to investigate the roles of CGRP in ocular vascular disease.

Observation of pathological retinal angiogenesis in the OIR model revealed no difference between CGRP-/- and wild-type (WT) mice. However, much higher levels of the CGRP receptor were present in the choroid than the retina. Then using laser-induced choroidal neovascularization (CNV), a model of exudative age-related macular degeneration (AMD), we found that CNV lesions are more severe in CGRP-/- than WT mice, and fluorescein angiography showed that leakage from CNV is greater in CGRP-/-. In addition, macrophage infiltration and TNF-α production were enhanced within the CNV lesions in CGRP-/- mice, and the TNF-α in turn suppressed the barrier formation of retinal pigment epithelial cells. *In vivo*, CGRP administration suppressed CNV formation, and CGRP also dose-dependently suppressed TNF-α production by isolated macrophages.

From these data, we conclude that CGRP suppresses the development of leaky CNV through negative regulation of inflammation. CGRP may thus be a promising therapeutic agent for the treatment of ocular vascular diseases associated with inflammation.

Introduction

In acquired blindness, retinal or choroidal neovascularization (CNV) is the main causative factor. Retinal neovascularization is induced by retinal hypoxia and is observed in diabetic retinopathy, retinal vein occlusion and retinopathy of prematurity. CNV occurs as a result of abnormalities in Bruch's membrane and the retinal pigment epithelium (RPE) [1] and is observed in exudative age-related macular degeneration (AMD), angioid streaks and high myopia.

Calcitonin gene-related peptide (CGRP) is a 37-amino acid peptide produced by alternative splicing of the primary transcript of the calcitonin/CGRP gene. CGRP was originally identified as a sensory neurotransmitter [2], and is now known to be structurally similar to the angiogenic factor adrenomedullin (AM) [3]. Moreover, CGRP and AM share the same receptor, calcitonin receptor-like receptor (CLR), a seven transmembrane G protein-coupled receptor [4]. The affinity of CLR for CGRP or AM is determined by three accessory proteins called receptor activity-modifying proteins (RAMP1-3) [4]. When associated with RAMP1, CLR has high affinity for CGRP; association with RAMP2 or RAMP3 gives CLR a high affinity for AM. Through analysis of knockout mice, we were able to demonstrate the novel angiogenic functions of AM and RAMP2 [5-8]. Recently, CGRP was also reported to possess angiogenic functionality [9-12]. The precise roles of CGRP in ocular vascular development and disease remain totally unknown, however.

To investigate pathological angiogenesis in the eye, two major animal models are frequently applied: the oxygen-induced retinopathy (OIR) model, which is designed to investigate retinal neovascularization under hypoxic exposure, and the laser-induced CNV model, which is recognized as a model of exudative AMD. Both models are characterized by uncontrolled production of fragile and leaky capillaries in the retina.

In OIR, the transition from hyperoxia to normoxia causes relative ischemia within the retina, which may be the precursor of pathological angiogenesis. On the other hand, both angiogenic and inflammatory processes play important roles in the pathophysiology of CNV. Interestingly, evidence now suggests that CGRP may be involved in the regulation of inflammatory responses [13 14], and thus could be involved in the ocular neovascularization associated with inflammation.

In the present study, therefore, we investigated the pathophysiological activities of endogenous CGRP in retinal and choroidal neovascularization. For this purpose, we induced OIR or CNV in CGRP knockout (CGRP-/-) mice.

Materials and Methods

Experimental animals

CGRP-/- mice were generated in our group using a targeting DNA construct that replaced exon 5 encoding a CGRP-specific region [15]. The CGRP-/- strain was on a pure C57BL/6J background and had undergone backcross breeding to C57BL/6J using the speed congenic method.

All animal handling procedures were in accordance with a protocol approved by the ethics committee of Shinshu University School of Medicine. All experiments were performed in accordance with the Association for Research in Vision and Ophthalmology's Statement for the Use of Animals in Ophthalmic and Vision Research and our institutional guidelines.

Physiological angiogenesis in neonates

On postnatal day 7 (P7) and P10, mice were evaluated using flat-mounted specimens of retina stained with isolectin B4 (isolectin GS-IB4 from Griffonia simplicifolia, Alexa Fluor 594 conjugate I21413; 1:200 dilution; Invitrogen, Carlsbad, CA). Superficial vascular development in the retina was quantified on P7, and deep vascular development was evaluated on P10. Vascular progression was measured by defining a straight line from the angiogenic front to the center of the retina for each retinal quadrant under low magnification. The number of vessel branches and the vessel density in the area near the developing vascular front on P7 were quantified in 400 μm x 400 μm fields.

Oxygen-induced retinopathy (OIR) model

Ischemic retinopathy and pathological neovascularization were induced using the OIR model established by Smith et al. [16]. Beginning on P7, mice were exposed to 75% oxygen for 5 days (P12) and then allowed to recover in room air to induce retinal neovascularization. Retinal angiogenesis was quantified as described previously with slight modification [17]. Briefly, on P17 the eyes were fixed in 4% paraformaldehyde (PFA) for 1 h at 4°C and then washed with PBS. Retinas were then isolated and stained overnight at 4°C with Alexa Fluor 594-conjugated Griffonia bandeiraea simplicifolia isolectin B4 in phosphate-buffered saline (PBS) with 0.3% Triton X-100. After washing three times in PBS, the retinas were whole-mounted onto microscope slides with the photoreceptor side down and then embedded in fluorescent mounting medium (Dako, Denmark). Images of whole-mount retinas were taken at 40× magnification using a fluorescence microscope (BZ-9000, Keyence, Japan). Avascular zones and neovascular tuft formation (regarded as pathological angiogenesis) were quantified using digital imaging/photo editing software (Adobe Photoshop CS5; Adobe Systems, San Jose, CA).

Laser-induced choroid neovascularization (CNV) model

Male mice between 9 and 12 weeks of age were used. After mice were anesthetized by intraperitoneal injection of 2,2,2-tribromoethanol (240 mg/kg; Wako, Osaka, Japan), the pupil was dilated with 1 drop of 0.5% tropicamide and 0.5% phenylephrine (Mydrine P, Santen, Osaka, Japan). CNV was then induced as described previously with some modification [18]. Laser injury was induced using a slit-lamp delivery system (GYC-1000; NIDEK, Gamagori, Japan) with a cover slip serving as a contact lens. The wavelength was 532 nm, the power was 200 mW, the duration was 50 ms, and the spot size was 50 μm. In each eye, four laser spots were

placed around the optic disk. Only eyes that exhibited subretinal bubbles, which indicated rupture of the Bruch membrane, were used for studies.

One day or 3, 7 days after laser injury, RPE-choroid-sclera complexes (choroidal complexes) were isolated for real-time reverse transcription-polymerase chain reaction (real-time PCR).

Fluorescein isothiocyanate-dextran perfusion and choroidal flat-mount

The sizes of the CNV lesions were measured in RPE-choroid-sclera flat-mounts (choroidal flat-mounts) as previously described [19]. On day 14 after laser application, mice were anesthetized and perfused with 1 ml of PBS containing 50 mg/ml fluorescein-labeled dextran (MW $2x10^6$) (FITC-dextran; Sigma-Aldrich) via the left ventricle. The eyes were then enucleated and fixed for 1 h in 4% paraformaldehyde, after which the cornea and lens were removed, and the entire retina was carefully dissected from the eyecup. Four radial cuts were then made from the edge to the equator, and the eyecup with the choroidal complex was flat-mounted with the sclera facing down and examined using a fluorescence microscope. The area of CNV in the choroidal flat-mounts was then measured using an image analysis application (BZ-H2A; Keyence, Japan). CNV lesions were identified as fluorescent blood vessels at the choroidal/retinal interface circumscribed by regions lacking fluorescence, which were measured as the laser photocoagulation scar area.

Immunohistochemistry of CLR and CGRP in retinal sections

For immunohistochemistry of CLR, we used WT albino mice (BALB/c) to observe the staining of pigment epithelia. The eyes were enucleated and fixed in 4% paraformaldehyde for 1h at 4°C, washed with PBS, and then embedded in paraffin.

Ten-μm-thick cross sections were deparaffinized and immunostained using polyclonal antibodies raised against CLR (1:200, rabbit; Bioss). After rinsing with PBS, the sections were incubated with Alexa Fluor 568-labeled secondary antibodies. For immunohistochemistry of CGRP, we used eyes from WT C57Bl6/J mice soon (within 10min) after the laser radiation. The sections were immunostained using polyclonal antibodies raised against CGRP (1:300, rabbit; Sigma). The sections were incubated with Alexa Fluor 488-labeled secondary antibodies. Images were obtained with a BZ-9000 microscope (Keyence).

Fluorescein angiography

In the laser-induced CNV model, fluorescein angiography (FA) was performed 14 days after the laser injury. To evaluate vascular leakage, we photographed the fluorescence at early (2-3 min) and late (5-6 min) times after intraperitoneal injection of 0.1 ml of 2.5% fluorescein (Alcon, Tokyo, JAPAN), and compared the severity of the leakage between them. We graded the severity of the leakage as described previously [20]: Grade 0, no fluorescence; Grade 1, no increase of fluorescent area or intensity between the two times; Grade 2A, increase in fluorescent intensity between the two times; Grade 2B, increase of both fluorescent area and intensity between the two times. These criteria are summarized in Table 2.

Immunostaining and counting macrophages infiltrating into CNV

To investigate the effect of CGRP-deficiency on macrophage infiltration, macrophages infiltrating into CNV lesions were counted. Seven days after the laser photocoagulation, mice were sacrificed and choroidal flat-mounts were made as described above. After blocking with 1% bovine serum albumin, the flat-mounts were

stained with rat anti-mouse F4/80 antibody (BIO-RAD, Hercules, CA) and Alexa 568-conjugated secondary antibody. The immunostained preparations were then examined using a fluorescence microscope, and F4/80-positive cells around CNV were counted.

Continuous administration of CGRP and CGRP antagonist to mice

Human αCGRP (Peptide Institute, Inc., Osaka, Japan) and its antagonist, αCGRP 8-37 (Peptide Institute) dissolved in PBS were infused into the subcutaneous tissues of WT mice at a rate of 50 nM/day using osmotic pumps (Alzet, DURECT Co., Cupertino, CA). The delivery rate was 0.5 μl/h, and the mice received αCGRP or αCGRP 8-37 for 7 to 14 days. One day after implantation of the pumps, mice were subjected to laser injury. Mice treated with PBS served as controls. CNV area was evaluated 14 days after and macrophage infiltration was evaluated 7 days after the laser injury.

Administration of lenalidomide to mice

CGRP-/- and WT mice were intraperitoneally injected with lenalidomide (Chemscene Chemicals, Monmouth Junction, NJ) at a dose of 10 mg/kg/day from a day before to 3 days after the laser photocoagulation. The dose and administration method were determined according to a previous study [21]. Mice treated with PBS served as controls. Seven days after the laser injury, CNV area and macrophage infiltration were evaluated.

Cell preparation

ARPE-19 human RPE cells were purchased from the American Type Culture Collection (ATCC, Manassas, VA). For preparation of isolated macrophages, mice

were intraperitoneally injected with 2 ml of 3% thioglycolate medium (DIFCO) (Biobrás, Montes Claros, Brazil). Three days later, macrophages were harvested by peritoneal lavage using cold PBS and placed in culture. In some cases, lipopolysaccharide (LPS) (Sigma-Aldrich) and/or human αCGRP (Peptide Institute Inc., Osaka, Japan) were used to stimulate and/or suppress cytokine production by the cultured macrophages.

RNA extraction and quantitative real-time RT-PCR analysis

Total RNA was extracted using Trizol Reagent (Invitrogen, Carlsbad, CA), after which the extracted RNA was treated with DNA-Free (Ambion, Austin, TX) to remove contaminating DNA, and 2-μg samples were reverse transcribed using a High Capacity cDNA Reverse Transcription Kit (Applied Biosystems, Carlsbad, CA). Quantitative real-time RT-PCR was carried out using an Applied Biosystems 7300 real time PCR System (Applied Biosystems) with SYBR green (Toyobo, Japan) or Realtime PCR Master Mix (Toyobo) and TaqMan probe (MBL). Values were normalized to mouse GAPDH (Pre-Developed TaqMan assay reagents, Applied Biosystems). The primers and probes used are listed in Table 1.

ELSA for quantifying TNF-α

TNF-α production by macrophages isolated from mice was quantified using specific enzyme-linked immunosorbent assay (ELISA) kits (R&D Systems, Minneapolis, MN) according to the manufacturer's instructions. To evaluate the suppressive effect of CGRP on cytokine production by macrophages stimulated for 4 h with 100 ng/ml LPS, 10^{-7}-10^{-10} M CGRP was added to the cells 1 h prior to the assay.

Observation of tight-junctions between RPE cells

ARPE-90 human RPE cells were grown until confluent and further cultured for 24 h with or without TNF-α (0.2-20 ng/ml). To visualize the tight-junctions between RPE cells, we immunostained the cells using anti-ZO-1 antibody (BD Biosciences-Pharmingen).

Statistical analysis

Values are expressed as means ± SEM. Student's t test and one-way analysis of variance, followed by Fisher's PLSD were used to evaluate the significance of differences. Values of $P < 0.05$ were considered significant.

Results

CGRP-/- neonates showed no apparent abnormalities in retinal vessel development

We initially compared the developing retinal vessels on P7 and P10 between WT and CGRP-/- neonates. On P7, the retinal vessels were elongating from the center of the retina toward the periphery in the superficial layer. Examination of lectin-stained whole retinas (Figure 1A) revealed that vascular progression did not differ between CGRP-/- and WT mice (Figure 1B). On P10, the vascular progression had reached the periphery of the retina; at that point, the vessels elongated into deeper layers. We detected no difference in the deep vessel progression between CGRP-/- and WT mice (Figure1C, D). We also quantified vessel density (Figure1E, F) and vessel branching on P7 (Figure1E, G) and found no significant differences between the two genotypes. These results indicate that retinal vessel development under physiological condition is unaffected by CGRP deficiency.

CGRP-/- and WT neonates showed no apparent differences in hypoxia-induced retinopathy

We next evaluated whether ischemia within the eyes evoke changes in retinal angiogenesis in CGRP-/- mice, as CGRP deficiency reportedly retarded angiogenesis in an ischemia model [9]. In the OIR model, mice were exposed to 75% oxygen for 5 days, from P7 to P12. During this period (hyperoxic phase) oxygen-induced loss of retinal vessels (vaso-obliteration) occurs. Then after the mice are returned to normoxic conditions (room air) for 5 days, from P12 to P17 (hypoxic phase), the hyperoxia-induced vessel loss leads to pathological angiogenesis. Both WT and CGRP-/- mice exposed to hyperoxia exhibited avascular zones in the central region of the retina on P12 (Figure 2A), and we detected no significant differences in the size of

the avascular zones between the two groups (Figure 2B). When we analyzed the retinas at the end of the hypoxic phase (P17), the avascular zones were similarly diminished due to progressive neovascularization in both groups (Figure 2C, D). On P17, we detected neovascular tuft formation. This aneurysmal formation of retinal arteries is typical of pathological angiogenesis and did not differ between WT and CGRP-/- mice (Figure 2E, F). These results are strikingly different from those obtained with heterozygous AM knockout (AM+/-) mice, which showed enlargement of the avascular zone and enhanced pathological angiogenesis [22]. Collectively, the similarity between the CGRP-/- and WT (CGRP+/+) phenotypes, and the difference between the CGRP-/- and AM+/- phenotypes demonstrate that CGRP has little, if any, involvement in hypoxia-induced retinal neovascularization.

CGRP receptor system is more abundant in the choroid than the retina

We next analyzed the distribution of CGRP and its receptor system within the eyes. Real-time RT-PCR analysis of the retina and choroid from WT mice revealed levels of CGRP expression to be equivalent in the two layers. On the other hand, the expression levels of CLR and RAMP1 (the CGRP receptor system) were, respectively, about 19-fold and 8-fold higher in the choroid than the retina. This prompted us to speculate that CGRP is much more involved in the physiology of the choroid than the retina.

Enhanced laser-induced CNV in CGRP-/- mice

Because it is known to be a sensory neurotransmitter, we hypothesized that CGRP would be most strongly involved in angiogenesis within regions of the eye where sensory nerve terminals are present, such as the choroid. To test that idea, we applied

a laser-induced CNV model of exudative AMD to WT and CGRP-/- mice. Examination of choroidal flat-mounts revealed that on day 14 after the laser injury, CGRP-/- mice showed significantly larger areas of CNV (23,458 ± 1679 μm^2) than WT mice (17,232 ± 1122 μm^2) (Figure 4A, B). Although the laser photocoagulation scar area did not differ between the two genotypes (Figure 4C), the CNV area-to-laser scar area ratio was significantly higher in CGRP-/- than WT mice (Figure 4D). This suggests that, with the same degree of laser-injury, there was greater neovascularization in CGRP-/- than WT mice.

CGRP and its receptor components in the choroid

To confirm the involvement of CGRP in laser-induced CNV, we analyzed the localization of CGRP and its receptor in sections of retina. Immunostaining was able to detect expression of the CGRP receptor CLR at the pigment epithelium (Figure 5A). The expression of CGRP was not clearly observed in the control mice, however, soon (within 10 minutes) after the laser radiation, we could detect a high level of immunostaining of CGRP at the laser irradiated area (Figure 5B). We think that tissue injury after the laser radiation may enhance the secretion of CGRP from nerve endings at the choroid.

Fluorescent angiography (FA) revealed enhanced leakage from CNV in CGRP-/- mice

To determine the severity of the CNV lesions, we analyzed the leakage from the CNV by performing FA on day 14 after the laser injury. Figure 6 shows typical fluorescence images obtained at earlier (2-3 min; Figure 6A) and later (5-6 min; Figure 6B) times after fluorescein injection. Using FA, we detected angiographic leakage

from CNV lesions in both genotypes, but CGRP-/- mice developed larger and leakier CNV lesions than did WT mice (Figure 6C). In particular, the numbers of grade 2B lesions (see Table 2 for definitions) were about 2-fold higher in CGRP-/- than WT mice. These results demonstrate that, in CGRP-/- mice, not only is laser-induced CNV formation enhanced, the lesions are much leakier and fragile than in WT mice.

Macrophage infiltration is enhanced in CGRP-/- mice after laser injury

Both angiogenesis and inflammation contribute to the pathophysiology of CNV. In earlier studies, we and others [14, 23, 24] clarified the role of CGRP in the regulation of inflammation. We therefore used immunohistological analysis to assess inflammatory cell invasion in choroidal flat-mounts on day 7 after laser injury. We found increased infiltration of F4/80-positive macrophages around the laser-irradiated area (Figure 7A), and the number of infiltrating macrophages was significantly greater in CGRP-/- than WT mice (Figure 7B).

On day 3 and 7 after the laser injury, real-time PCR analysis showed significantly higher TNF-α mRNA level in the choroidal complex of CGRP-/- than WT mice (Figure 7C). Thus the inflammatory response appears to be greater in CGRP-/- than WT mice.

CGRP suppresses TNF-α expression by macrophages

Given that endogenous CGRP appears to suppress inflammation caused by the laser injury, we next analyzed the effect of CGRP-administration on the production of inflammatory cytokines by macrophages. Stimulating cultured macrophages with LPS upregulated expression of TNF-α, but that effect was suppressed by prior CGRP administration (Figure 8A). Moreover, CGRP administration dose-dependently suppressed TNF-α protein level in macrophage-conditioned cultured medium (Figure

8B).

Tight junctions between RPE cells are disrupted by TNF-α

Evidence suggests that the inflammatory cytokines produced by macrophages infiltrating laser injury-induced lesions can disrupt the barrier integrity of RPE cells [25]. In the present study, we initially confirmed that ARPE-19 cultured human RPE cells express TNF-α receptor, TNFR1 (Figure 9A). Then using confluent monolayers of cultured RPE cells, we detected expression of the tight junction molecule, ZO-1, between the RPE cells, and further observed that administration of TNF-α dose-dependently disrupted the tight junction formation, as indicated by the ZO-1 distribution (Figure 9B).

Exogenous administration of CGRP suppresses CNV formation

To directly evaluate the ability of exogenous CGRP to suppress CNV formation, we used osmotic pumps to continuously administer CGRP to mice. One day after the start of CGRP-administration, mice were subjected to laser injury. Under these conditions, we found that mice receiving CGRP showed substantially less CNV formation and less macrophage infiltration (Figure 10A-C) than control mice. In contrast, administration of CGRP 8-37 (CGRP antagonist) increased macrophage infiltration.

Effect of TNF-α inhibition on enhanced CNV formation and macrophage invasion in CGRP-/- mice.

Finally, we analyzed the effect of intraperitoneal administration of lenalidomide, which suppresses TNF-α production. We evaluated the effect of this TNF-α inhibitor

on the enhanced CNV formation and macrophage infiltration observed in CGRP-/- mice. As expected, in CGRP-/-, lenalidomide treatment suppressed the CNV formation and macrophage infiltration to levels similar to those observed in WT mice. (Figure 11A-D).

Discussion

In the present study, we investigated the physiological and pathological roles of endogenous CGRP in the eye. CGRP-/- neonates showed no apparent changes in physiological retinal vessel development or hypoxia-induced retinopathy, as compared to WT neonates. Like AM, CGRP reportedly exhibits angiogenic activity in various diseases models [9-12]. In addition, CGRP has been shown to promote the proliferation and migration of vascular endothelial cells [26] via AMP-activated protein kinase [27]. *In vivo*, the angiogenic effect of CGRP has been observed in tissues and organs that contain sensory nerves [9, 10]. We therefore speculated that CGRP is likely involved in angiogenesis within the eye, particularly in regions where sensory nerve terminals are abundant – e.g., in the ciliary body, choroid and ocular surface.

Within the eye, CGRP is present in the terminals of sensory nerve fibers branching from the trigeminal nerve. The choroid possesses numerous CGRP(+) intrinsic choroidal neurons, which are observed in the suprachoroid. These neurons are more numerous in the temporal than in the nasal regions, especially in the central choroid underneath the macular area of the retina [28]. Furthermore, we found strong expression of the CGRP receptor components CLR and RAMP1 in the choroid. These observations prompted us to use FA to examine the role of CGRP in a laser-induced CNV model, which is recognized as a model of exudative AMD. Notably, CNV lesions were significantly larger and leakier in CGRP-/- than WT mice.

At a glance, enhanced CNV formation in CGRP-/- mice would seem to be contradictory, given the reported angiogenic functions of CGRP [9-12]. Similar conflicting results were also obtained with AM, though the angiogenic functions of AM have now been confirmed [5, 6]. Furthermore, we recently reported that mice deficient in AM show less pathological angiogenesis in the OIR model [22]. By contrast, Yuda et al.

reported that pathological angiogenesis in the laser-induced CNV model is enhanced in AM knockout mice [29]. The discrepancy between these results likely reflects the different pathogenesis of OIR and CNV. The primary force driving retinal angiogenesis in OIR is hypoxia, whereas it appears to be chronic inflammation in AMD [30]. Yuda et al. showed that AM administration inhibited macrophage infiltration and reduced CNV formation by suppressing chemokine production [29]. Consistent with those results, we and others have shown that AM exerts anti-inflammatory effects [31, 32].

In the pathogenesis of AMD, CNV formation is associated with macrophage accumulation [33, 34]. CGRP acts directly on macrophages and regulates their production of cytokines in lesions associated with chronic inflammation [24]. In the present study, we found that infiltration of macrophages and their accumulation within the laser-induced wounds was increased in CGRP-/- mice. In addition, CGRP-/- showed higher TNF-α expression in the choroidal complex than WT mice. Conversely, CGRP administration directly suppressed the production and secretion of TNF-α from isolated macrophages. These results clearly demonstrate that endogenous CGRP suppresses inflammatory reaction through negative regulation of macrophage infiltration and cytokine production. Given that pathological angiogenesis is closely related with inflammation[35], our findings suggest CGRP is involved in the pathophysiology of ocular neovascularization associated with inflammation.

In the laser-induced CNV model, the laser burn disrupts Bruch's membrane, and new vessels from the choroid invade the subretinal space, which destroys the architecture of the retina. These pathological vessels are fragile and leaky, and ultimately exacerbate the inflammation, stimulating further neovascularization from the choroid beyond the disrupted Bruch's membrane. This vicious cycle of angiogenesis and inflammation is damaging to the retina and eventually causes central vision loss [36].

Endogenous CGRP may work to break this vicious circle, thereby preventing the retinal damage.

In this study, we also analyzed the RPE, which exists between the retina and the choroid. The RPE is composed of a single layer of hexagonal cells with well-developed tight junctions, which control the molecular transport from the choroidal vessels and maintain the retinal environment. We found that administration of TNF-α disrupted the tight junctions between RPE cells. As CGRP appears to suppress TNF-α production from macrophages, it may also suppress CNV formation by contributing to the maintenance of RPE integrity. The illustration in Figure 12 summarizes the mechanism by which CGRP may exert its protective effect against laser-induced CNV. Macrophages infiltrating into CNV lesions, and enhance neovascular invasion from the choroid to the retina. These vessels are fragile and leaky, and further enhance the inflammation in the retina. Macrophages also damage the RPE barrier by disrupting tight junctions through production of TNF-α. CGRP is mainly produced by the terminals of sensory nerve, which is located at the choroid. Tissue injury after the laser radiation may enhance the secretion of CGRP from the nerve endings. CGRP then suppresses the macrophage invasion and, in turn, the pathological angiogenesis and disruption of RPE barrier function.

Exudative AMD is the primary cause of CNV in humans. As the populations of most developed countries are getting older, the incidence of AMD is growing [37] [38]. The molecular mechanism underlying the pathogenesis of AMD is not fully understood; however, VEGF is known to play a key role in ocular vascular diseases, and anti-angiogenic therapy using an anti-VEGF antibody that targets angiogenesis and diminishes vessel permeability is widely used to treat exudative AMD. Unfortunately, the anti-VEGF antibody is not sufficient to prevent eventual blindness in advanced

cases, so other therapeutic targets are being sought to inhibit the progression of pathological angiogenesis. In the present study, we suppressed laser-induced CNV formation and macrophage infiltration through exogenous administration of CGRP. Our findings suggest CGRP could potentially serve as a novel therapeutic agent with which to control ocular vascular disease.

Acknowledgements

This study was supported by the Funding Program for Next Generation World-Leading Researchers (NEXT Program) from the Cabinet Office, Government of Japan, a Grant-in-Aid for Scientific Research (KAKENHI), a research grant for Cardiovascular Diseases from the National Cardiovascular Center, and research grants from the Novartis Foundation for Gerontological Research, the Ichiro Kanehara Foundation, the Cosmetology Research Foundation, SENSHIN Medical Research Foundation, Nagao Memorial Fund, Kanzawa Medical Research Foundation, Ono Medical Research Foundation, the Nakatomi Foundation, the Japan Heart Foundation & Astellas/Pfizer Grant for Research on Atherosclerosis Update, the Research Foundation for Opto-Science and Technology, the Japan Vascular Disease Research Foundation, and Takeda Science Foundation.

Figure legends

Table 1

Primers and probes used for quantitative real-time RT-PCR and RT-PCR

Table 2

Grading of the severity of vascular leakage using fluorescent angiography (FA) after laser-induced CNV

Figure 1

Comparison of physiological angiogenesis in CGRP-/- and WT

(A) Representative lectin-stained flat-mount preparation showing the retinal vessels in WT and CGRP-/- mice on P7 (B) Bar graph comparing vessel progression in the superficial layer of the retina. Percent vessel progression was defined by a straight line from the angiogenic front to the center of the retina for each retinal quadrant under low magnification (40x). (C) Photomicrographs showing the deep vessel layer at the edge of a retinal quadrant from a WT and CGRP-/- mouse on P10. Scale bar = 100 μm. (D) Bar graph comparing percent vessel progression. (E) Photomicrographs showing areas near the developing vascular front on P7. Scale bar = 100 μm. (F, G) Bar graphs comparing the percent vessel density (F) and the number of vessel branches (G) per field between WT and CGRP-/- mice. Bars depict means ± SEM. Data are from 4 quadrants per retina from 4 mice. No apparent difference in physiological angiogenesis was detected between CGRP-/- and WT mice.

Figure 2

Evaluation of OIR-induced pathological angiogenesis in CGRP-/- and WT mice

(A) Representative P12 (soon after high-oxygen treatment) retinal flat-mount specimens with lectin staining. (B) Bar graph comparing the percent avascular zone in the whole retina on P12 between WT and CGRP-/- mice. n = 4 in each group. (C) Representative retinal flat-mount specimens from P17, at the end of room air treatment. (D) Bar graph comparing the percent avascular zone within the whole retina on P17. WT n = 12, CGRP-/- n = 11. (E) Neovascular tuft formation (retinal pathological angiogenesis) at the border of avascular zones on P17 in OIR model mice. Scale bar = 100 μm. (F) Bar graph comparing the percent neovascular tuft area within the whole retina. WT n = 12, CGRP-/- n = 11. Bars in (B), (D) and (F) depict means ± SEM. No difference in the areas of avascular zones or the degree of neovascular tuft formation was detected between CGRP-/- and WT mice.

Figure 3

Comparison of the gene expression of CGRP and its receptor system in retina and choroid

Bar graphs comparing the gene expression of CGRP, CLR and RAMP1. The expression level in the retina was assigned a value of 1. n = 5 in each group. Bars are means ± SEM. ***$p<0.001$. Levels of the CGRP receptor components, CLR and RAMP1, were much higher in the choroid than the retina.

Figure 4

Evaluation of choroid neovascularization (CNV) in the laser injury model

On day 14 after the laser-induced injury to Bruch's membrane, choroidal flat-mounts

were made, and the areas of FITC-positive CNV lesions were compared between CGRP-/- and WT mice. (A) Representative retinal flat-mount specimens after intraventricular injection of FITC-dextran. Scale bars = 100 μm. (B-D) Bar graphs comparing the areas of the CNV (B), laser scar (C) and the CNV area/laser scar area ratio (D). Bars are means ± SEM. n = 10 in each group, **p<0.01.

Figure 5

Expression of CGRP and its receptor in the choroid.

(A) Immunohistostaining of CLR, the CGRP receptor, in the pigment epithelium (shown by arrows) of a BALB/c WT mouse.

(B) Immunohistostaining of CGRP at the laser irradiated area soon (within 10 minutes) after the laser radiation in C57BL/6J mouse. We could detect high immunostaining of CGRP at the laser irradiated area (arrow). Bars = 50 μm.

Figure 6

Evaluation of leakage from CNV using fluorescein angiography (FA)

(A, B) Typical FA images obtained at the indicated times after fluorescein injection. Vascular leakage was evaluated using the grading scheme outlined in Table 2. (C) Representative FA of WT and CGRP-/- eyes, showing larger and leakier CNV lesions in the CGRP-/- eye. (D) Histogram showing the percentage of each CNV leakage grade among the eyes tested. Larger CNV lesions with greater leakage on FA developed in CGRP-/- than WT mice. n = 5 in each group.

Figure 7

Evaluation of macrophage infiltration and inflammatory gene expression

Macrophages, which accumulated within laser burns and around laser scars, were analyzed on day 7 after the laser injury. (A) Representative fluorescent immunostaining for the macrophage marker F4/80 (red) and DAPI (blue). Scale bars = 100 μm (B) Bar graphs comparing the numbers of macrophages. F4/80-positive cells inside or around each laser photocoagulation site were counted. **P<0.01. n = 4 in each. (C) Quantitative real-time PCR analysis of TNF-α expression in samples from choroidal complexes collected on day 1, 3, and 7 after laser injury. Data are shown as ratios when the level of WT control was assigned a value of 1. Each mouse without laser-induced CNV is shown as control. Bars are means ± SEM. **P<0.01. *P<0.05. n = 6 in day 1 and 7, n = 7 in day 3 in each mouse. CGRP-/- mice showed significantly greater infiltration of F4/80-positive macrophages and higher levels of TNF-α expression than WT mice.

Figure 8

Anti-inflammatory effects of CGRP on macrophages

(A) Quantitative real-time PCR analysis of macrophages isolated from WT mice. After stimulation for 4 h with LPS (100 mg/ml), expression of TNF-α was upregulated, but that effect was suppressed by addition of human αCGRP (10^{-7} M) 1 h prior to LPS stimulation. Data are shown as ratios when the expression of control (Ctrl; without LPS and CGRP) was assigned a value of 1. Bars are means ± SEM. *P<0.05. n = 6. (B) Results from ELISA quantifying TNF-α level in culture supernatants conditioned by macrophages. The macrophages were stimulated for 4 h with LPS (100 ng/ml), and CGRP (10^{-9}-10^{-7}M) was added 1 h prior to LPS-stimulation. CGRP dose-dependently suppressed the production of TNF-α by macrophages. Bars are means ± SEM. ***P< 0.001. n = 4 in each.

Figure 9

Effect of TNF-α on the tight junctions between RPE cells

(A) RT-PCR analysis showing the expression of TNFR1, the TNF-α receptor, in ARPE-19 cultured human RPE cells. (B) Immunostaining of ZO-1-positive tight junctions between cultured ARPE-19 cells. Bars = 50 μm. Administration of TNF-α to ARPE-19 cells dose-dependently enhanced disruption of ZO-1-positive tight junctions.

Figure 10

Effects of continuous administration of CGRP and CGRP-antagonist on the CNV formation

(A) Representative fluorescent image of FITC-positive CNV lesions (upper panel) and fluorescent immunostaining of macrophage marker F4/80 (red) and DAPI (blue) (lower panel) in control (PBS-treated), CGRP-treated, and CGRP 8-37 (CGRP antagonist)-treated WT mice. Bars = 100 μm. (B) Bar graphs comparing the areas of the CNV. (C) Bar graphs comparing the numbers of macrophages. Bars are means ± SEM. *$P<0.05$. n = 4 and 6 in (B) and (C), respectively. Mice receiving CGRP showed substantially less CNV formation and less macrophage infiltration than control mice.

Figure 11

Effect of TNF-α inhibition on enhanced CNV formation and macrophage invasion in CGRP-/- mice

Representative fluorescent image of FITC-positive CNV lesions (A) and fluorescent

immunostaining of macrophage marker F4/80 (red) and DAPI (blue) (C) in control (PBS-treated) and lenalidomide-treated WT and CGRP-/- mice. Bars = 100 μm. (B) Bar graphs comparing the areas of the CNV. (D) Bar graphs comparing the numbers of macrophages. Bars are means ± SEM. n = 5 in WT and n = 6 in CGRP-/-. In CGRP-/-, lenalidomide treatment suppressed the CNV formation and macrophage infiltration to levels similar to those observed in WT mice.

Figure 12

Illustration summarizing the protective effects of CGRP against CNV

References

[1] Lopez PF, Grossniklaus HE, Lambert HM, Aaberg TM, Capone A, Jr., Sternberg P, Jr., L'Hernault N: Pathologic features of surgically excised subretinal neovascular membranes in age-related macular degeneration. Am J Ophthalmol 1991, 112:647-56.

[2] Rosenfeld MG, Mermod JJ, Amara SG, Swanson LW, Sawchenko PE, Rivier J, Vale WW, Evans RM: Production of a novel neuropeptide encoded by the calcitonin gene via tissue-specific RNA processing. Nature 1983, 304:129-35.

[3] Kitamura K, Kangawa K, Kawamoto M, Ichiki Y, Nakamura S, Matsuo H, Eto T: Adrenomedullin: a novel hypotensive peptide isolated from human pheochromocytoma. Biochemical and biophysical research communications 1993, 192:553-60.

[4] McLatchie LM, Fraser NJ, Main MJ, Wise A, Brown J, Thompson N, Solari R, Lee MG, Foord SM: RAMPs regulate the transport and ligand specificity of the calcitonin-receptor-like receptor. Nature 1998, 393:333-9.

[5] Shindo T, Kurihara Y, Nishimatsu H, Moriyama N, Kakoki M, Wang Y, Imai Y, Ebihara A, Kuwaki T, Ju KH, Minamino N, Kangawa K, Ishikawa T, Fukuda M, Akimoto Y, Kawakami H, Imai T, Morita H, Yazaki Y, Nagai R, Hirata Y, Kurihara H: Vascular abnormalities and elevated blood pressure in mice lacking adrenomedullin gene. Circulation 2001, 104:1964-71.

[6] Iimuro S, Shindo T, Moriyama N, Amaki T, Niu P, Takeda N, Iwata H, Zhang Y, Ebihara A, Nagai R: Angiogenic effects of adrenomedullin in ischemia and tumor growth. Circ Res 2004, 95:415-23.

[7] Ichikawa-Shindo Y, Sakurai T, Kamiyoshi A, Kawate H, Iinuma N, Yoshizawa T, Koyama T, Fukuchi J, Iimuro S, Moriyama N, Kawakami H, Murata T, Kangawa K, Nagai R, Shindo T: The GPCR modulator protein RAMP2 is essential for angiogenesis and vascular integrity. J Clin Invest 2008, 118:29-39.

[8] Koyama T, Ochoa-Callejero L, Sakurai T, Kamiyoshi A, Ichikawa-Shindo Y, Iinuma N, Arai T, Yoshizawa T, Iesato Y, Lei Y, Uetake R, Okimura A, Yamauchi A, Tanaka M, Igarashi K, Toriyama Y, Kawate H, Adams RH, Kawakami H, Mochizuki N, Martinez A, Shindo T: Vascular endothelial adrenomedullin-RAMP2 system is essential for vascular integrity and organ homeostasis. Circulation 2013, 127:842-53.

[9] Mishima T, Ito Y, Hosono K, Tamura Y, Uchida Y, Hirata M, Suzsuki T, Amano H, Kato S, Kurihara Y, Kurihara H, Hayashi I, Watanabe M, Majima M: Calcitonin gene-related peptide facilitates revascularization during hindlimb ischemia in mice. American journal of physiology Heart and circulatory physiology 2011, 300:H431-9.

[10] Ohno T, Hattori Y, Komine R, Ae T, Mizuguchi S, Arai K, Saeki T, Suzuki T, Hosono K, Hayashi I, Oh-Hashi Y, Kurihara Y, Kurihara H, Amagase K, Okabe S, Saigenji K, Majima M: Roles of calcitonin gene-related peptide in maintenance of gastric mucosal integrity and in enhancement of ulcer healing and angiogenesis. Gastroenterology 2008, 134:215-25.

[11] Toda M, Suzuki T, Hosono K, Hayashi I, Hashiba S, Onuma Y, Amano H, Kurihara Y, Kurihara H, Okamoto H, Hoka S, Majima M: Neuronal system-dependent facilitation of tumor angiogenesis and tumor growth by calcitonin gene-related peptide. Proc Natl Acad Sci U S A 2008, 105:13550-5.

[12] Toda M, Suzuki T, Hosono K, Kurihara Y, Kurihara H, Hayashi I, Kitasato H, Hoka S, Majima M: Roles of calcitonin gene-related peptide in facilitation of wound healing and angiogenesis. Biomed Pharmacother 2008, 62:352-9.

[13] Matsuda R, Kezuka T, Nishiyama C, Usui Y, Matsunaga Y, Okunuki Y, Yamakawa N, Ogawa H, Okumura K, Goto H: Suppression of murine experimental autoimmune optic neuritis by mature dendritic cells transfected with calcitonin gene-related Peptide gene. Invest Ophthalmol Vis Sci 2012, 53:5475-85.

[14] Kamiyoshi A, Sakurai T, Ichikawa-Shindo Y, Fukuchi J, Kawate H, Muto S, Tagawa Y, Shindo T: Endogenous alphaCGRP protects against concanavalin A-induced hepatitis in mice. Biochem Biophys Res Commun 2006, 343:152-8.

[15] Oh-hashi Y, Shindo T, Kurihara Y, Imai T, Wang Y, Morita H, Imai Y, Kayaba Y, Nishimatsu H, Suematsu Y, Hirata Y, Yazaki Y, Nagai R, Kuwaki T, Kurihara H: Elevated sympathetic nervous activity in mice deficient in alphaCGRP. Circ Res 2001, 89:983-90.

[16] Smith LE, Wesolowski E, McLellan A, Kostyk SK, D'Amato R, Sullivan R, D'Amore PA: Oxygen-induced retinopathy in the mouse. Invest Ophthalmol Vis Sci 1994, 35:101-11.

[17] Connor KM, Krah NM, Dennison RJ, Aderman CM, Chen J, Guerin KI, Sapieha P, Stahl A, Willett KL, Smith LE: Quantification of oxygen-induced retinopathy in the mouse: a model of vessel loss, vessel regrowth and pathological angiogenesis. Nature protocols 2009, 4:1565-73.

[18] Izumi-Nagai K, Nagai N, Ozawa Y, Mihara M, Ohsugi Y, Kurihara T, Koto T, Satofuka S, Inoue M, Tsubota K, Okano H, Oike Y, Ishida S: Interleukin-6 receptor-mediated activation of signal transducer and activator of transcription-3 (STAT3) promotes choroidal neovascularization. Am J Pathol 2007, 170:2149-58.

[19] Yu HG, Liu X, Kiss S, Connolly E, Gragoudas ES, Michaud NA, Bulgakov OV, Adamian M, DeAngelis MM, Miller JW, Li T, Kim IK: Increased choroidal neovascularization following laser induction in mice lacking lysyl oxidase-like 1. Invest Ophthalmol Vis Sci 2008, 49:2599-605.

[20] Hoerster R, Muether PS, Vierkotten S, Schroder S, Kirchhof B, Fauser S: In-vivo and ex-vivo characterization of laser-induced choroidal neovascularization variability in mice. Graefes Arch Clin Exp Ophthalmol 2012, 250:1579-86.

[21] Rozewski DM, Herman SE, Towns WH, 2nd, Mahoney E, Stefanovski MR, Shin JD, Yang X, Gao Y, Li X, Jarjoura D, Byrd JC, Johnson AJ, Phelps MA: Pharmacokinetics and tissue disposition of lenalidomide in mice. AAPS J 2012, 14:872-82.

[22] Iesato Y, Toriyama Y, Sakurai T, Kamiyoshi A, Ichikawa-Shindo Y, Kawate H, Yoshizawa T, Koyama T, Uetake R, Yang L, Yamauchi A, Tanaka M, Igarashi K, Murata T, Shindo T: Adrenomedullin-RAMP2 system is crucially involved in retinal angiogenesis. Am J Pathol 2013, 182:2380-90.

[23] Kamiyoshi A, Sakurai T, Ichikawa-Shindo Y, Iinuma N, Kawate H, Yoshizawa T, Koyama T, Muto S, Shindo T: Endogenous alpha-calcitonin gene-related peptide mitigates liver fibrosis in chronic hepatitis induced by repeated administration of concanavalin A. Liver Int 2009, 29:642-9.

[24] Holzmann B: Antiinflammatory activities of CGRP modulating innate immune responses in health and disease. Curr Protein Pept Sci 2013, 14:268-74.

[25] Penfold PL, Madigan MC, Gillies MC, Provis JM: Immunological and aetiological aspects of macular degeneration. Progress in retinal and eye research 2001, 20:385-414.

[26] Mapp PI, McWilliams DF, Turley MJ, Hargin E, Walsh DA: A role for the sensory neuropeptide calcitonin gene-related peptide in endothelial cell proliferation in vivo. Br J Pharmacol 2012, 166:1261-71.

[27] Zheng S, Li W, Xu M, Bai X, Zhou Z, Han J, Shyy JY, Wang X: Calcitonin gene-related peptide promotes angiogenesis via AMP-activated protein kinase. Am J Physiol Cell Physiol 2010, 299:C1485-92.

[28] de Hoz R, Ramirez AI, Salazar JJ, Rojas B, Ramirez JM, Trivino A: Substance P and calcitonin gene-related peptide intrinsic choroidal neurons in human choroidal whole-mounts. Histol Histopathol 2008, 23:1249-58.

[29] Yuda K, Takahashi H, Inoue T, Ueta T, Iriyama A, Kadonosono K, Tamaki Y, Aburatani H, Nagai R, Yanagi Y: Adrenomedullin inhibits choroidal neovascularization via CCL2 in the retinal pigment epithelium. Am J Pathol 2012, 181:1464-72.

[30] Hollyfield JG, Bonilha VL, Rayborn ME, Yang X, Shadrach KG, Lu L, Ufret RL, Salomon RG, Perez VL: Oxidative damage-induced inflammation initiates age-related macular degeneration. Nat Med 2008, 14:194-8.

[31] Niu P, Shindo T, Iwata H, Iimuro S, Takeda N, Zhang Y, Ebihara A, Suematsu Y, Kangawa K, Hirata Y, Nagai R: Protective effects of endogenous adrenomedullin on cardiac hypertrophy, fibrosis, and renal damage. Circulation 2004, 109:1789-94.

[32] Ashizuka S, Inagaki-Ohara K, Kuwasako K, Kato J, Inatsu H, Kitamura K: Adrenomedullin treatment reduces intestinal inflammation and maintains epithelial barrier function in mice administered dextran sulphate sodium. Microbiology and immunology 2009, 53:573-81.

[33] Khandhadia S, Cipriani V, Yates JR, Lotery AJ: Age-related macular degeneration and the complement system. Immunobiology 2012, 217:127-46.

[34] Luhmann UF, Robbie S, Munro PM, Barker SE, Duran Y, Luong V, Fitzke FW, Bainbridge JW, Ali RR, MacLaren RE: The drusenlike phenotype in aging Ccl2-knockout mice is caused by an accelerated accumulation of swollen autofluorescent subretinal macrophages. Investigative ophthalmology & visual science 2009, 50:5934-43.

[35] Mor F, Quintana FJ, Cohen IR: Angiogenesis-inflammation cross-talk: vascular endothelial growth factor is secreted by activated T cells and induces Th1 polarization. Journal of immunology 2004, 172:4618-23.

[36] Malchiodi-Albedi F, Matteucci A, Bernardo A, Minghetti L: PPAR-gamma, Microglial Cells, and Ocular Inflammation: New Venues for Potential Therapeutic

Approaches. PPAR research 2008, 2008:295784.

[37] Yasuda M, Kiyohara Y, Hata Y, Arakawa S, Yonemoto K, Doi Y, Iida M, Ishibashi T: Nine-year incidence and risk factors for age-related macular degeneration in a defined Japanese population the Hisayama study. Ophthalmology 2009, 116:2135-40.

[38] Kawasaki R, Yasuda M, Song SJ, Chen SJ, Jonas JB, Wang JJ, Mitchell P, Wong TY: The prevalence of age-related macular degeneration in Asians: a systematic review and meta-analysis. Ophthalmology 2010, 117:921-7.

Primers and probes used for quantitative real-time RT-PCR

mCGRP Forward	5’-GGAGCAGGAGGAAGAGCAG-3’
mCGRP Reverse	5’-TGCCAGCCGATGGGTCACA-3’
mCLR Forward	5’-AGGCGTTTACCTGCACACACT-3’
mCLR Reverse	5’-CAGGAAGCAGAGGAAACCCC-3’
mCLR Probe	5’-ATCGTGGTGGCTGTGTTTGCGGAG-3’
mRAMP1 Forward	5’-GCACTGGTGGTCTGGAGGA-3’
mRAMP1 Reverse	5’-CCCTCATCACCTGGGATACCT-3’
mRAMP1 Probe	5’-CAAGCGCACAGAGGGCATCGTG-3’
mTNF-α Forward	5’-ACGGCATGGATCTCAAAGAC-3’
mTNF-α Reverse	5’-AGATAGCAAATCGGCTGACG-3’

Primers used for RT-PCR

hTNFR1 Forward	5’-GGTGCTAACCCCTCGATGTA-3’
hTNFR1 Reverse	5’-GCTTGCTATGTGCTTGTCCA-3’

Table 1

Grading of the severity of vascular leakage using fluorescent angiography (FA) after laser-induced CNV

Grade 0 No fluorescence
Grade1 No increase of fluorescent area or intensity between the two times
Grade2A Increase in fluorescent intensity between the two times
Grade2B Increase of both fluorescent area and intensity between the two times

Table 2

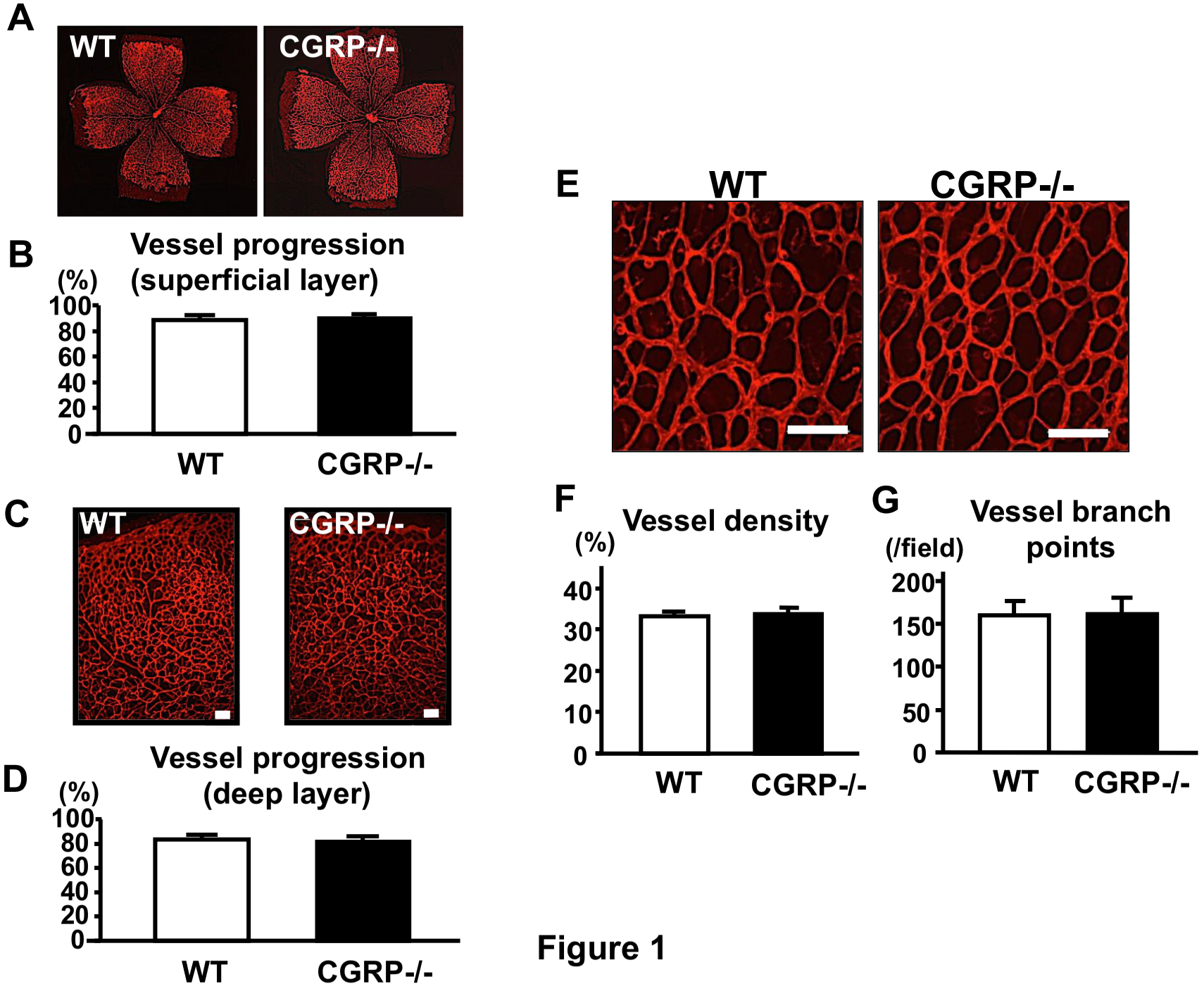
A
WT
CGRP-/-
B
Vessel progression
(superficial layer)
(%)
100
80
60
40
20
0
WT
CGRP-/-
C
WT
CGRP-/-
D
Vessel progression
(deep layer)
(%)
100
80
60
40
20
0
WT
CGRP-/-
E
WT
CGRP-/-
F
Vessel density
(%)
40
30
20
10
0
WT
CGRP-/-
G
Vessel branch
points
(/field)
200
150
100
50
0
WT
CGRP-/-

Figure 1

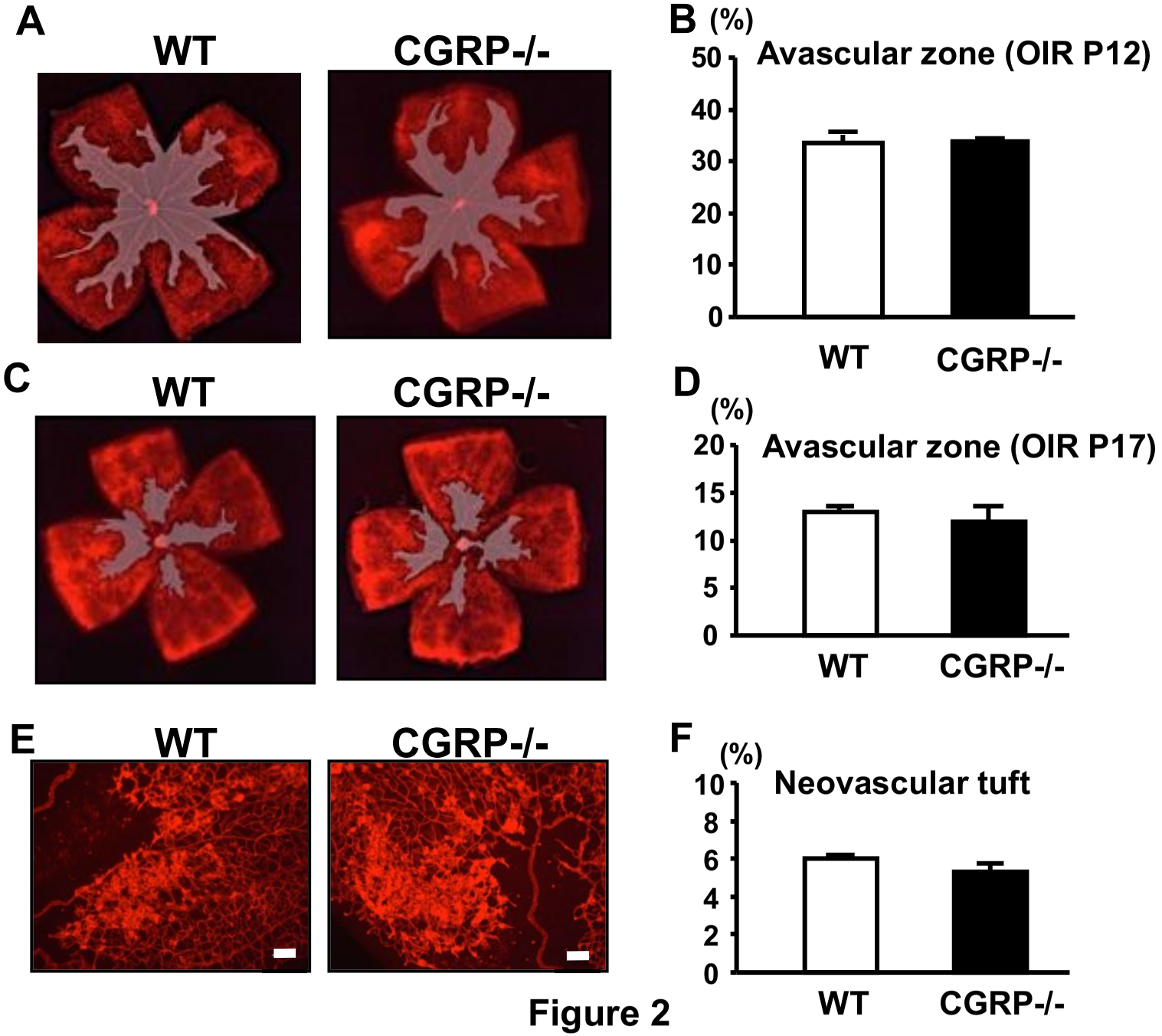
A
WT
CGRP-/-
B
(%)
Avascular zone (OIR P12)
50
40
30
20
10
0
WT
CGRP-/-
C
WT
CGRP-/-
D
(%)
Avascular zone (OIR P17)
20
15
10
5
0
WT
CGRP-/-
E
WT
CGRP-/-
F
(%)
Neovascular tuft
10
8
6
4
2
0
WT
CGRP-/-

Figure 2

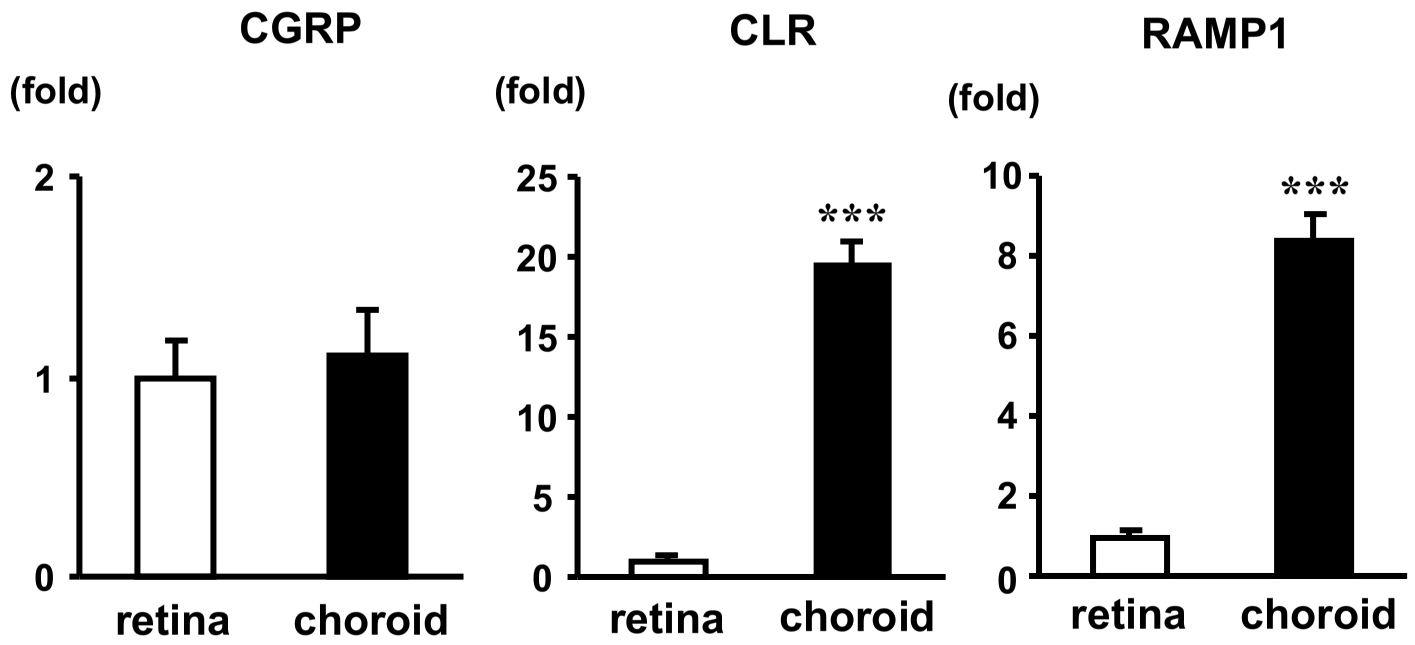
CGRP
(fold)
2
1
0
retina
choroid
CLR
(fold)
25
20
15
10
5
0
***
retina
choroid
RAMP1
(fold)
10
8
6
4
2
0
***
retina
choroid

Figure 3

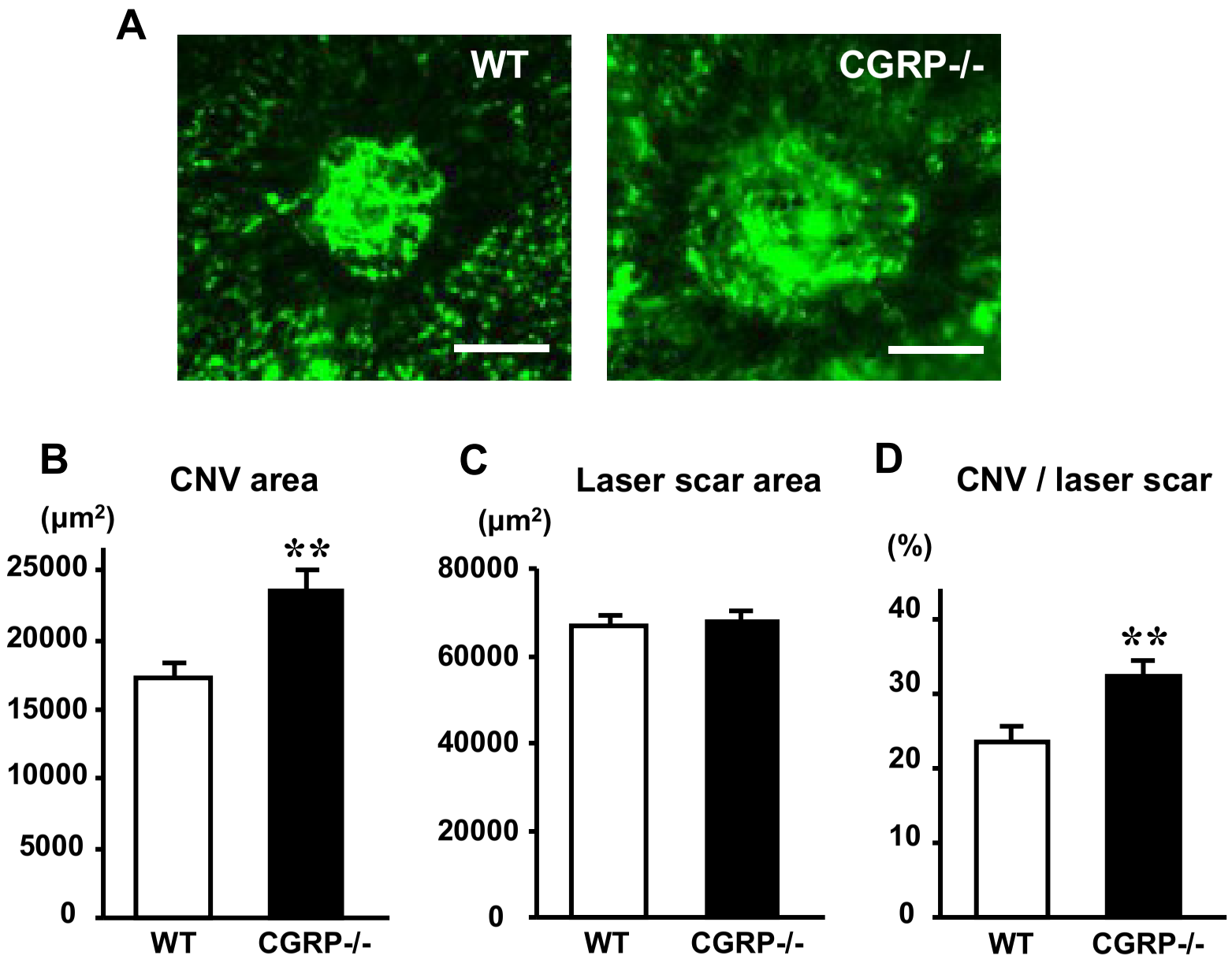
A
WT
CGRP-/-
B
CNV area
(μm²)
25000
20000
15000
10000
5000
0
**
WT
CGRP-/-
C
Laser scar area
(μm²)
80000
60000
40000
20000
0
WT
CGRP-/-
D
CNV / laser scar
(%)
40
30
20
10
0
**
WT
CGRP-/-

Figure 4

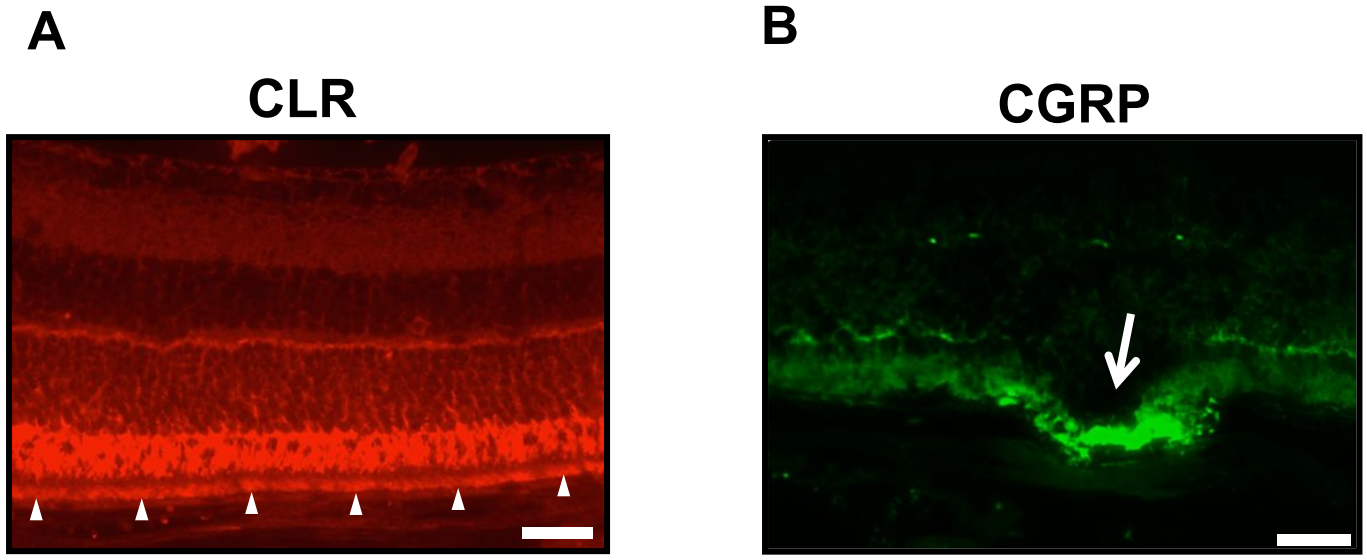

Figure 5

A

Earlier time (2～3min)

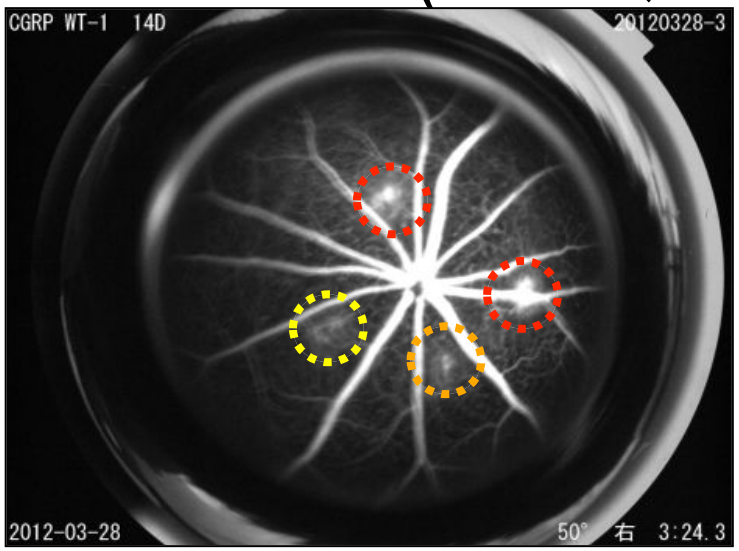

B

Later time（5～6min)

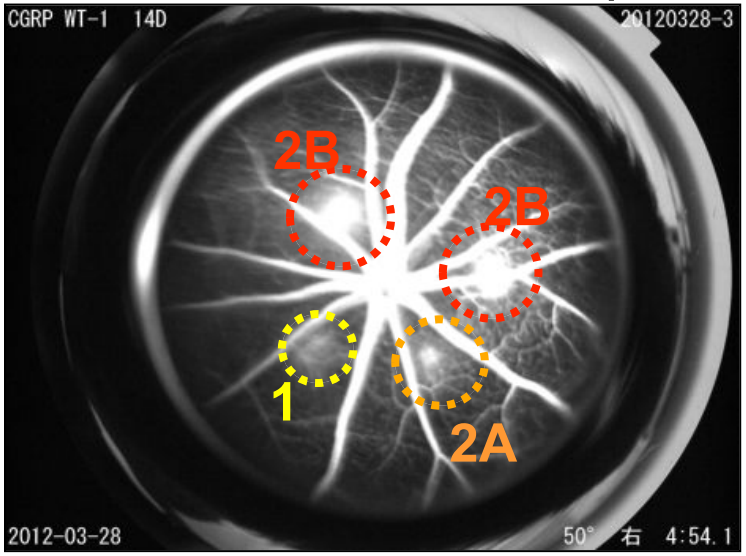

C

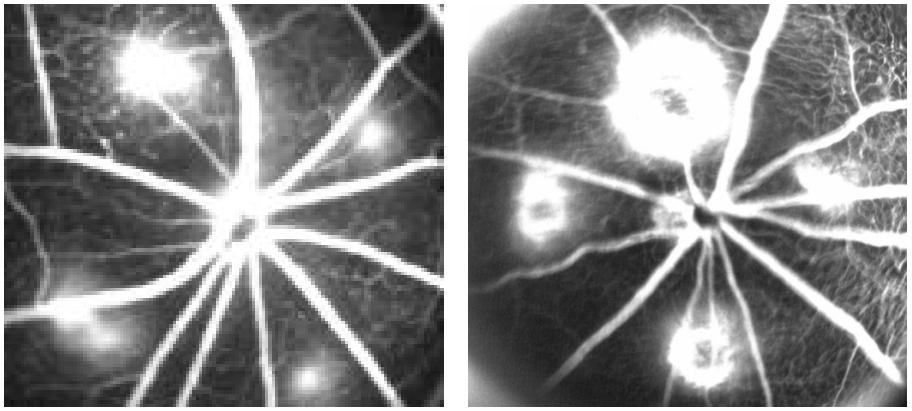

D

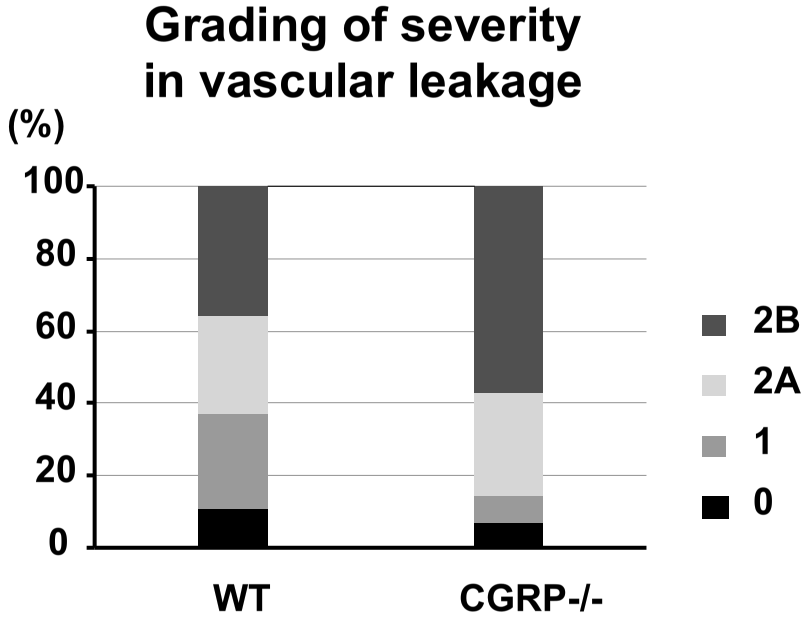

Figure 6

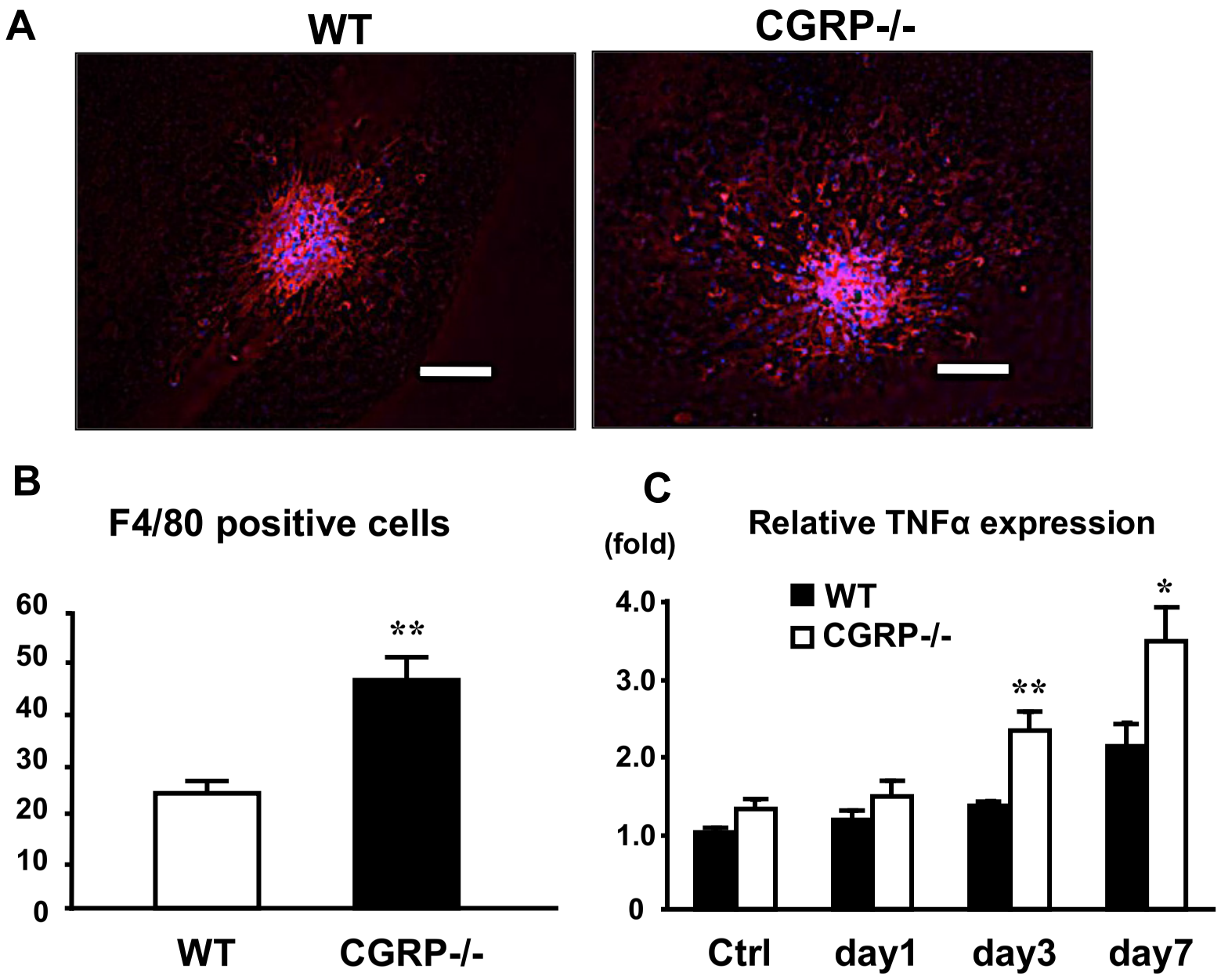
A
WT
CGRP-/-
B
F4/80 positive cells
60
50
40
30
20
10
0
**
WT
CGRP-/-
C
(fold)
Relative TNFα expression
WT
CGRP-/-
4.0
3.0
2.0
1.0
0
*
**
Ctrl
day1
day3
day7

Figure 7

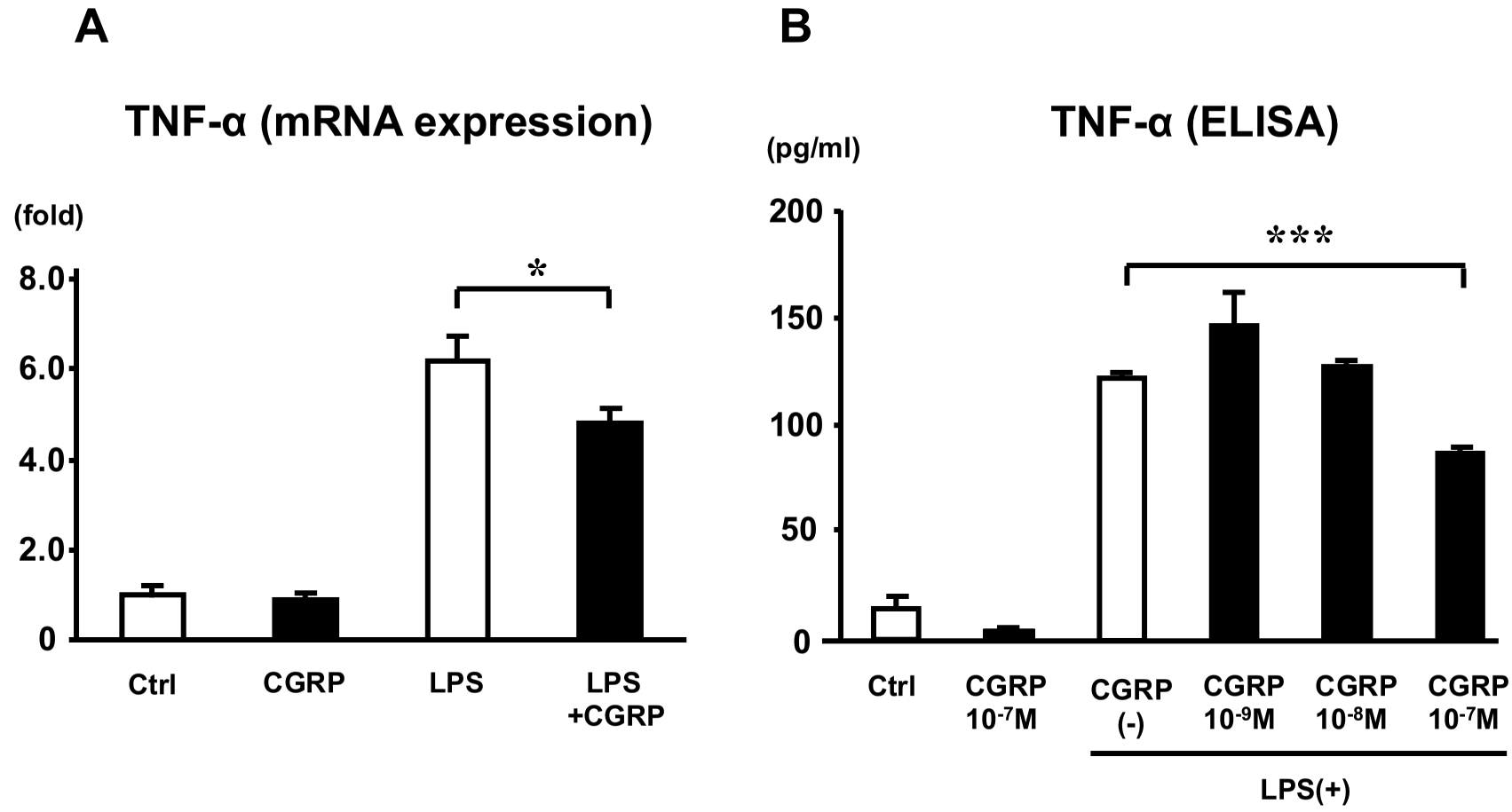
A
TNF-α (mRNA expression)
(fold)
8.0
6.0
4.0
2.0
0
*
Ctrl
CGRP
LPS
LPS
+CGRP
B
TNF-α (ELISA)
(pg/ml)
200
150
100
50
0
***
Ctrl
CGRP
10-7M
CGRP
(-)
CGRP
10-9M
CGRP
10-8M
CGRP
10-7M
LPS(+)

Figure 8

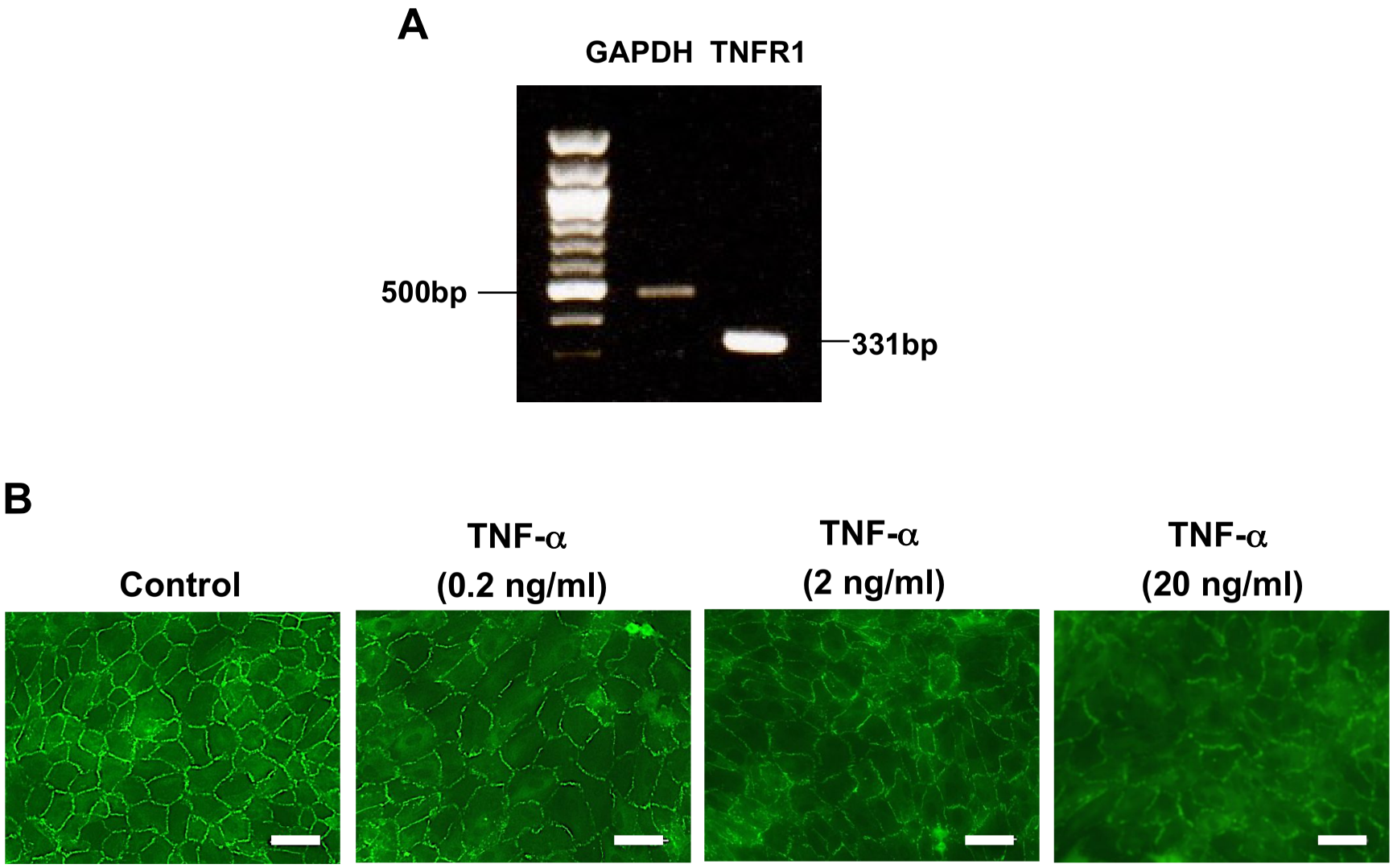
A
GAPDH
TNFR1
500bp
331bp
B
Control
TNF-α
(0.2 ng/ml)
TNF-α
(2 ng/ml)
TNF-α
(20 ng/ml)

Figure 9

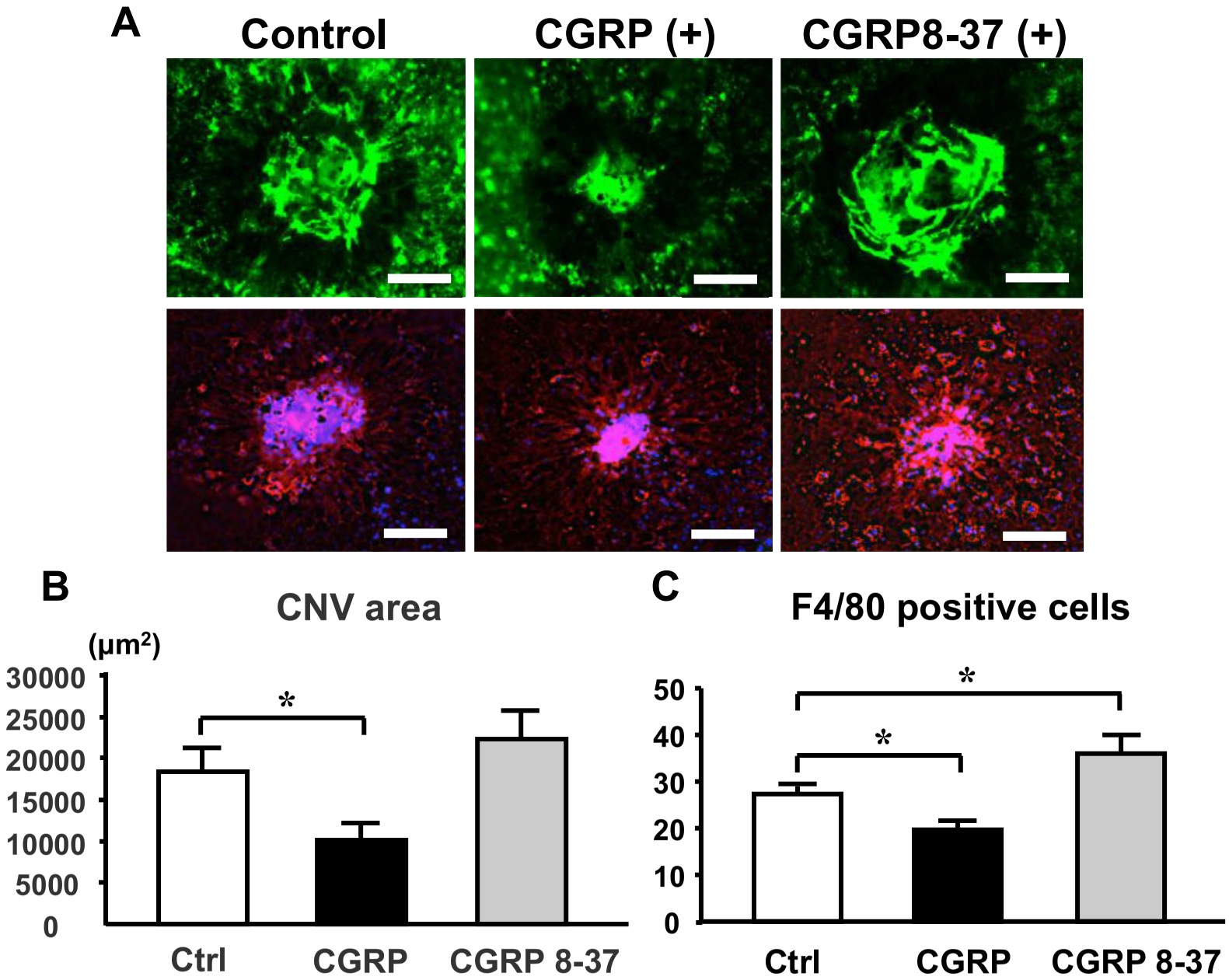
A
Control
CGRP (+)
CGRP8-37 (+)
B
CNV area
(μm²)
30000
25000
20000
15000
10000
5000
0
*
Ctrl
CGRP
CGRP 8-37
C
F4/80 positive cells
50
40
30
20
10
0
*
*
Ctrl
CGRP
CGRP 8-37

Figure 10

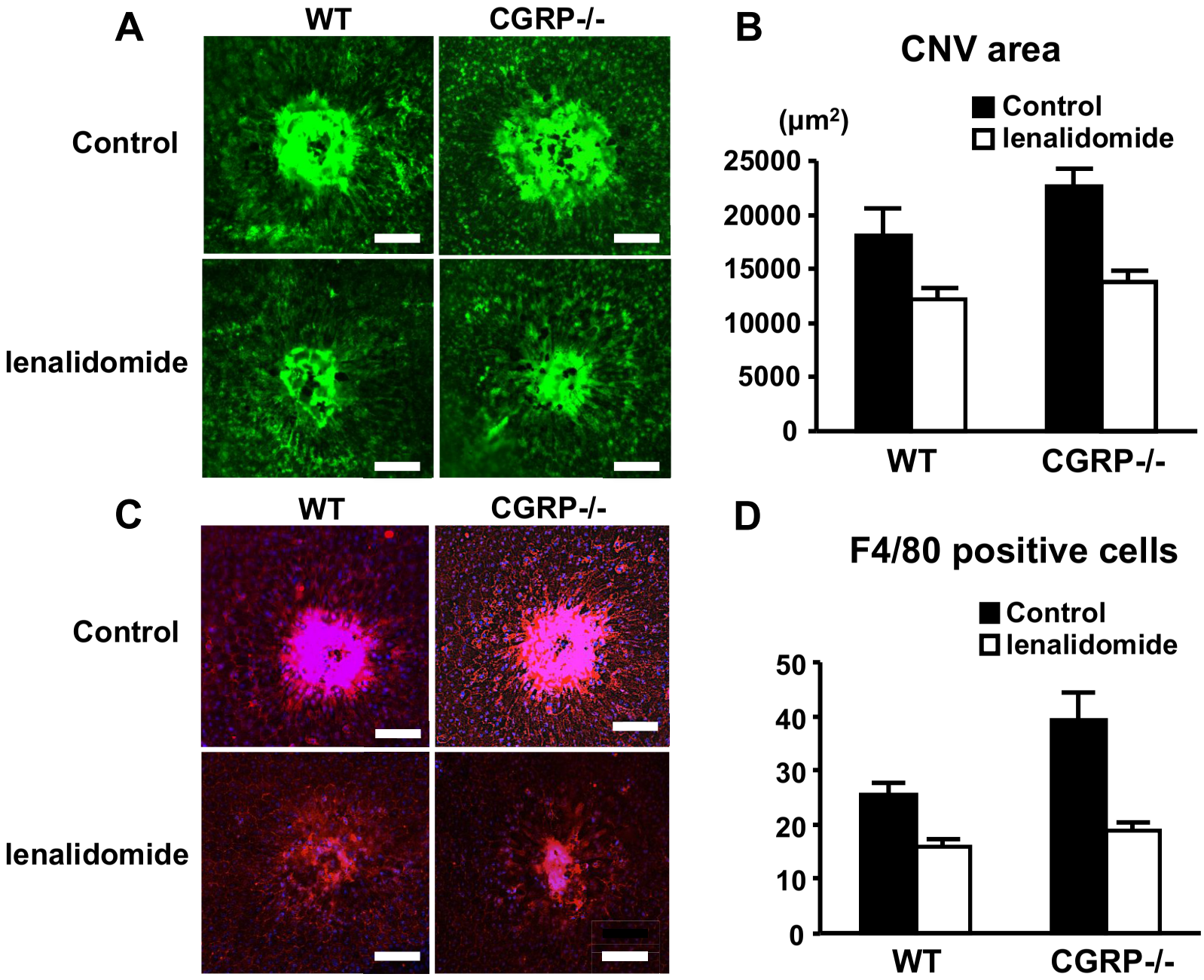
A
WT
CGRP-/-
Control
lenalidomide
B
CNV area
(μm²)
Control
lenalidomide
25000
20000
15000
10000
5000
0
WT
CGRP-/-
C
WT
CGRP-/-
Control
lenalidomide
D
F4/80 positive cells
Control
lenalidomide
50
40
30
20
10
0
WT
CGRP-/-

Figure 11

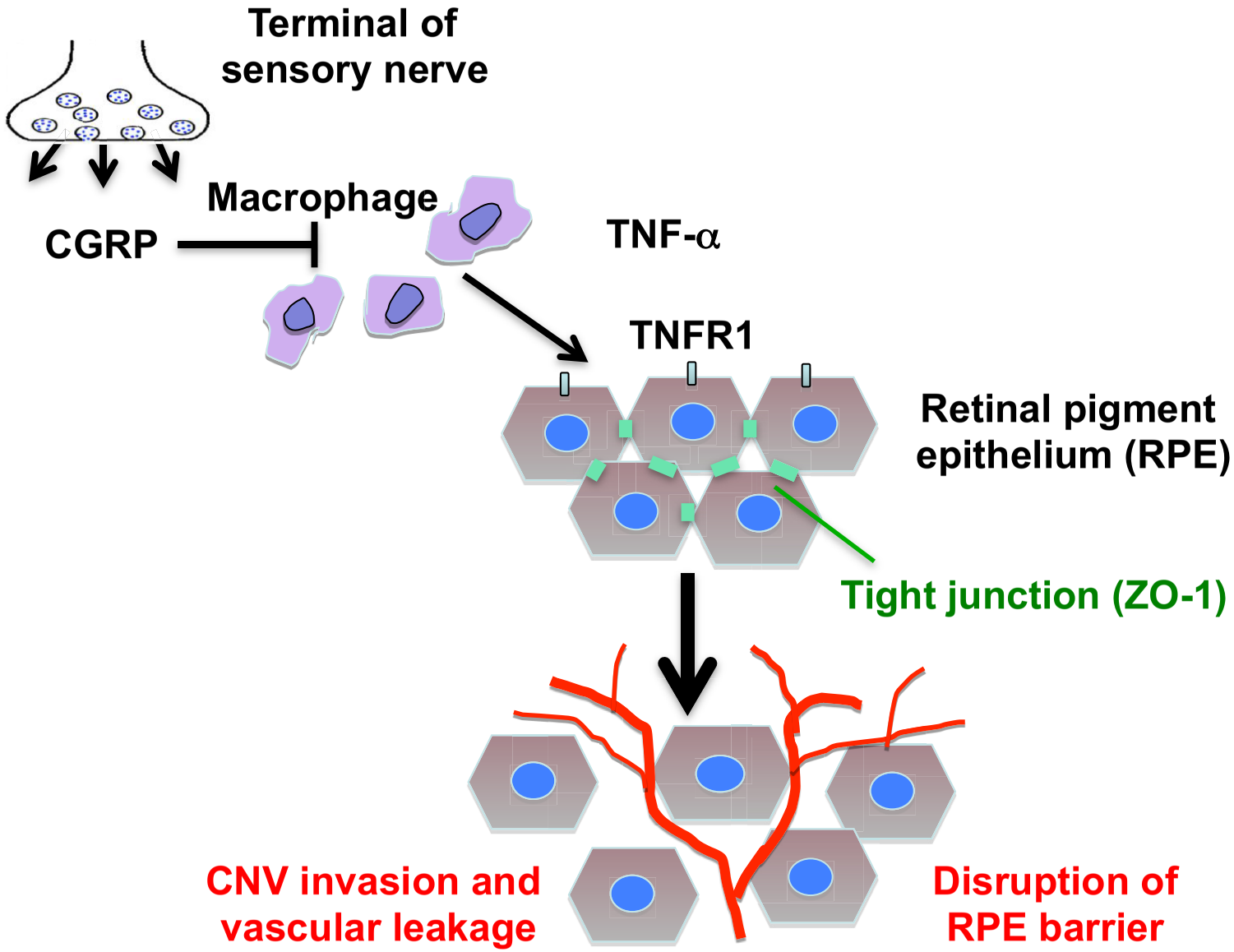
Terminal of
sensory nerve
Macrophage
CGRP
TNF-α
TNFR1
Retinal pigment
epithelium (RPE)
Tight junction (ZO-1)
CNV invasion and
vascular leakage
Disruption of
RPE barrier

Figure 12

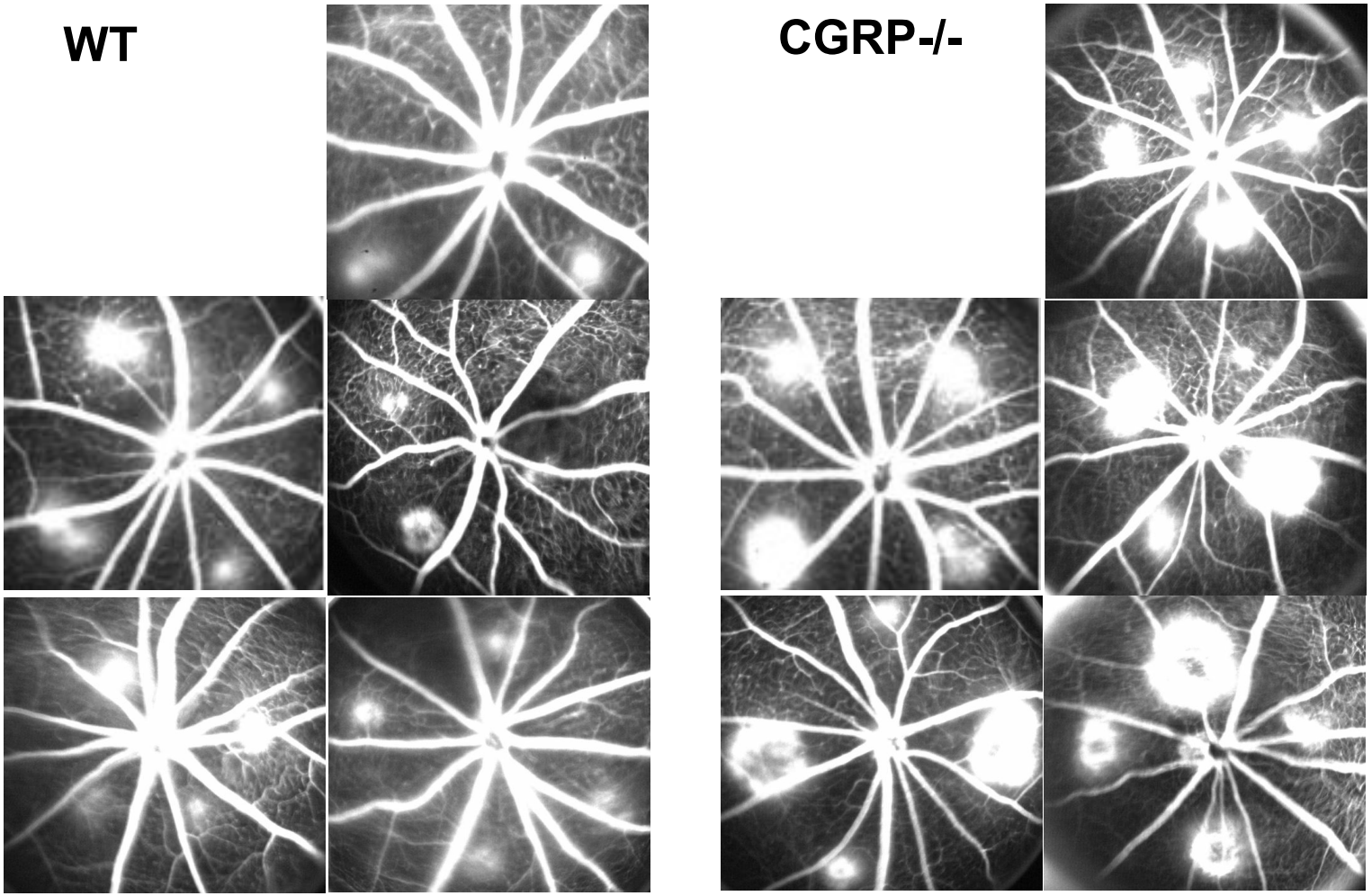

Supplementary Figure 1

FFA images (n=5) used for assessment of CNV grade in this study.
Larger CNV lesions with greater leakage on FA developed in CGRP-/- compared to WT mice.

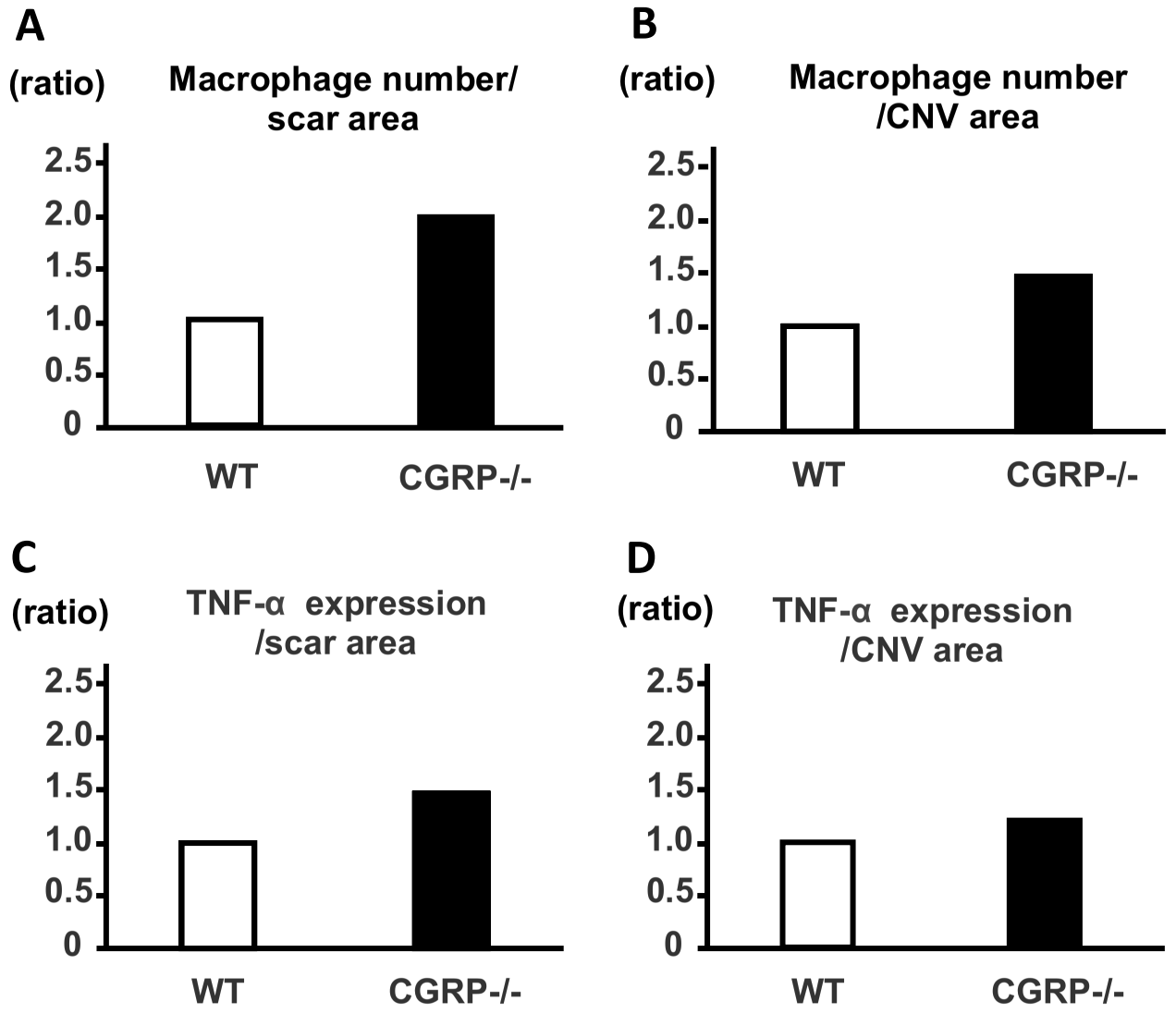

Supplementary Figure 2

(A, B) Bar graph comparing infiltrating macrophage number normalized by the scar and CNV area, respectively. (C, D) Bar graph comparing TNF-α gene expression normalized by scar and CNV area, respectively. The level in the WT was assigned a value of 1. Macrophage infiltration and TNF-α expression were analyzed at day 7 of CNV injury. Bars are means ± SEM. n = 5 in each group.

```
CLUSTAL 2.1 Multiple Sequence Alignments
Sequence type explicitly set to DNA
Sequence format is Pearson
Sequence 1: Human         387 bp
Sequence 2: Mouse         387 bp
Start of Pairwise alignments
Aligning...

Sequences (1:2) Aligned. Score: 79.3282
Guide tree file created:
```

```
Human  ATGGGCTTCCAAAAGTTCTCCCCCTTCCTGGCTCTCAGCATCTTGGTCCTGTTGCAGGCA
Mouse  ATGGGCTTCCTGAAGTTCTCCCCTTTCCTGGTTGTCAGCATCTTGCTCCTGTACCAGGCA
       **********  ********** ******* * ********** ******  ******

Human  GGCAGCCTCCATGCAGCACCATTCAGGTCTGCCCTGGAGAGCAGCCCAGCAGACCCGGCC
Mouse  TGCAGCCTCCAGGCAGTGCCTTTGAGGTCAATCTTGGAAAGCAGCCCA---GGCATGGCC
        ********** ****  ** ** *****   * **** *********   * *  ****

Human  ACGCTCAGTGAGGACGAAGCGCGCCTCCTGCTGGCTGCACTGGTGCAGGACTATGTGCAG
Mouse  ACTCTCAGTGAAGAAGAAGTTCGC---CTGCTGGCTGCACTGGTGCAGGACTATATGCAG
       ** ******** ** ****  ***   ************************** *****

Human  ATGAAGGCCAGTGAGCTGGAGCAGGAGCAAGAGAGAGAGG------GCTCCAGAATCATT
Mouse  ATGAAAGCCAGGGAGCTGGAGCAGGAGGAAGAGCAGGAGGCTGAGGGCTCTAGTGTCACT
       ***** ***** ************** *****   ****      **** **  *** *

Human  GCCCAGAAGAGAGCCTGTGACACTGCCACCTGTGTGACTCATCGGCTGGCAGGCTTGCTG
Mouse  GCTCAGAAGAGATCCTGCAACACTGCCACCTGTGTGACCCATCGGCTGGCAGGTCTGCTG
       ** ********* ****  ****************** **************  *****

Human  AGCAGATCAGGGGGTGTGGTGAAGAACAACTTTGTGCCCACCAATGTGGGTTCCAAAGCC
Mouse  AGCAGATCAGGAGGTGTGGTGAAGGACAACTTTGTTCCCACCAATGTGGGCTCTGAAGCC
       ********** ********** ********** ************** **  *****

Human  TTTGGCAGGCGCCGCAGGGACCTTCAAGCCTGA
Mouse  TTCGGCCGCCGCCGCAGGGACCTTCAGGCCTGA
       ** *** * ********** ******
```

NM_001289444 Mus musculus calcitonin/calcitonin-related polypeptide, alpha (Calca), transcript variant 3, mRNA

NM_001033953 Homo sapiens calcitonin-related polypeptide alpha (CALCA), transcript variant 3, mRNA

Supplementary Figure 3

Sequence alignment of human and mouse αCGRP

Homology of human and mouse αGRP is about 80%.

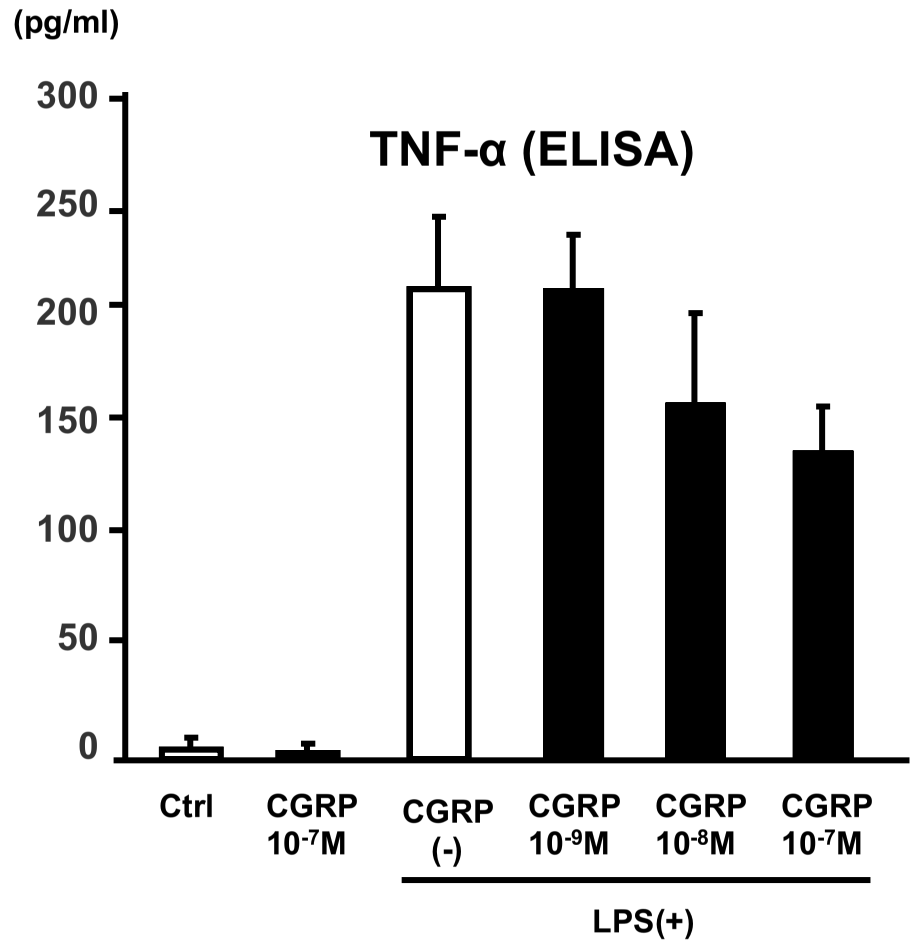

Supplementary Figure 4

Effect of rat αCGRP on LPS-stimulated TNF-α production by macrophages

After stimulation for 4 h with LPS (100 mg/ml), expression of TNF-α was upregulated, but the effect was suppressed by addition of rat αCGRP 1 h prior to LPS stimulation. Data are shown as ratios when the expression of control (Ctrl; without LPS and CGRP) was assigned a value of 1. Bars are means ± SEM. n = 8. The macrophages were stimulated for 4 h with LPS (100 ng/ml), and CGRP (10^{-9}-10^{-7}M) was added 1 h prior to LPS-stimulation. CGRP dose-dependently suppressed the production of TNF-α by macrophages.

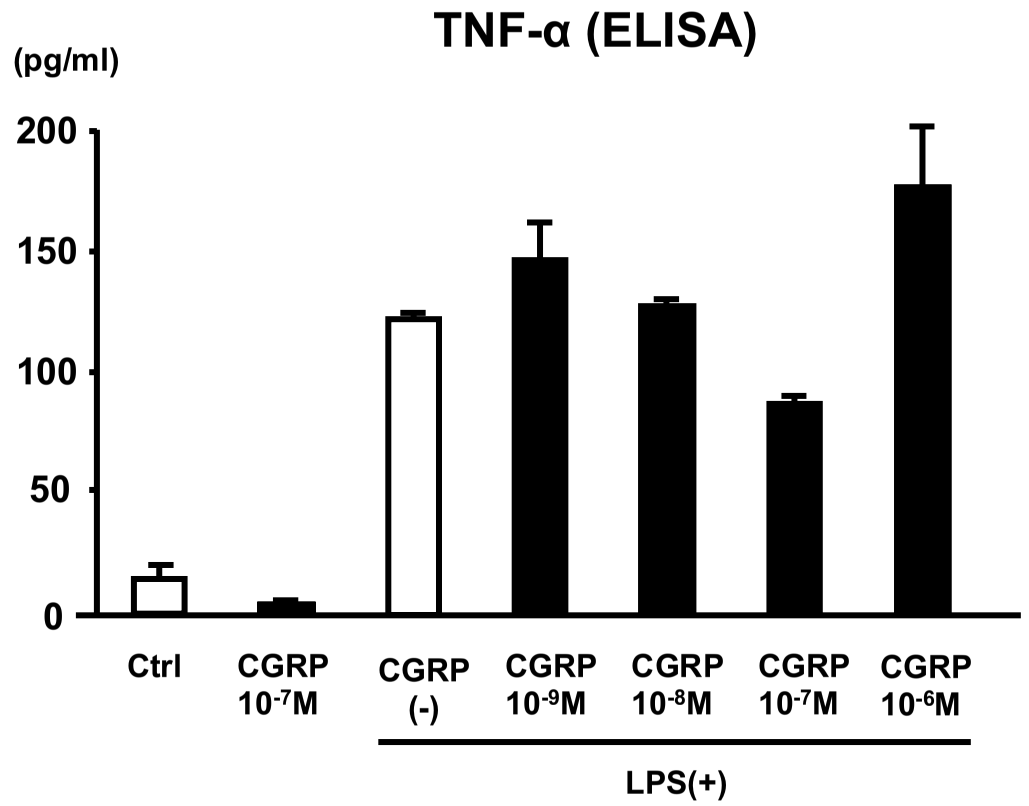

Supplementary Figure 5

Effect of higher dosage of human αCGRP on LPS-stimulated TNF-α production by macrophages
Lower dose of human αCGRP dose-dependently suppressed LPS（100 ng/ml）-stimulated TNF-α production. Bars are means ± SEM. n = 8. The macrophages were stimulated for 4 h with LPS (100 ng/ml), and CGRP (10^{-9}-10^{-7}M) was added 1 h prior to LPS-stimulation. Interestingly, a higher dose of CGRP (>10^{-6}M) caused elevation of TNF-α production by the macrophages.

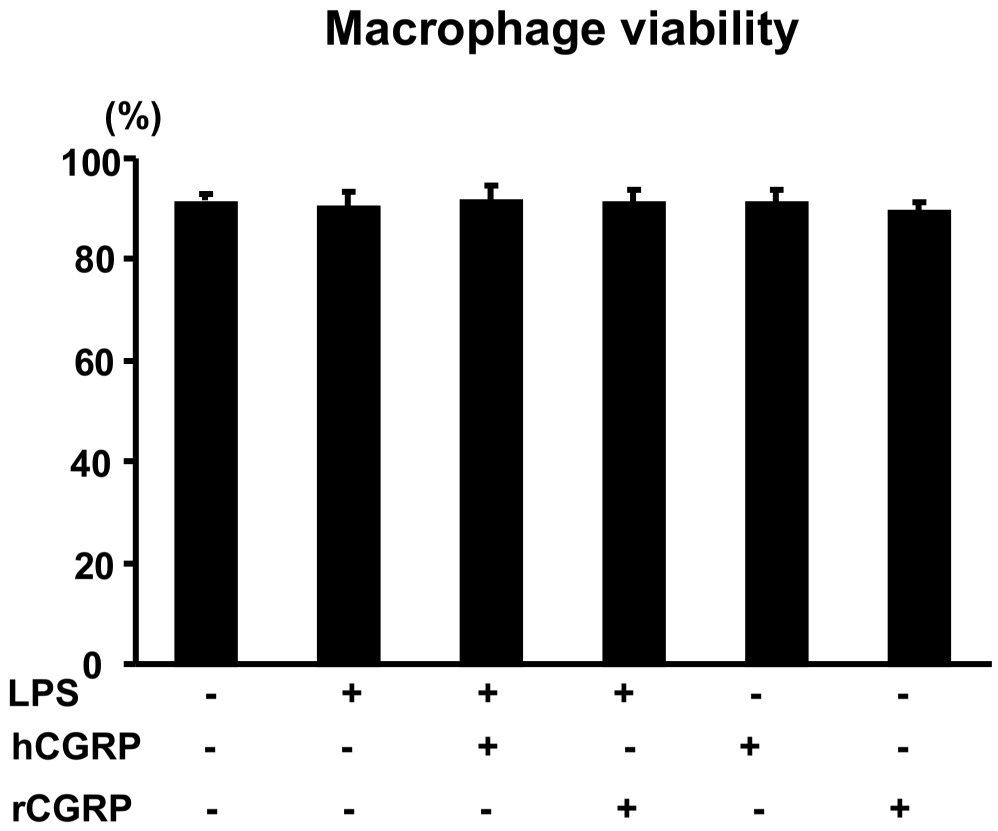

Supplementary Figure 6

Stimulation of macrophages with LPS and/or CGRP did not affect cellular viability
Viability of macrophages was analyzed with or without LPS and/or CGRP stimulation. For the LPS stimulation, macrophages were incubated for 4 h with LPS (100 mg/ml). For the CGRP stimulation, macrophages were incubated with human or rat CGRP (10^{-7} M) from 1 h prior to the LPS stimulation. After propidium iodide staining, the percentage of living macrophages was counted. Bars depict means ± SEM. n = 8.

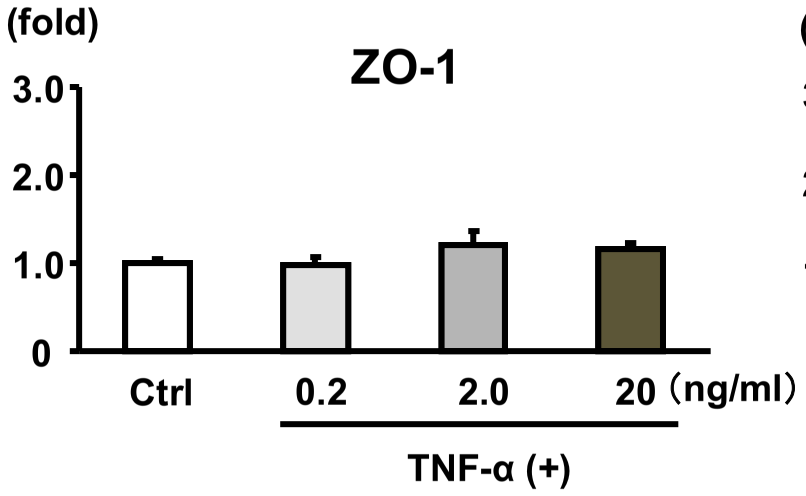

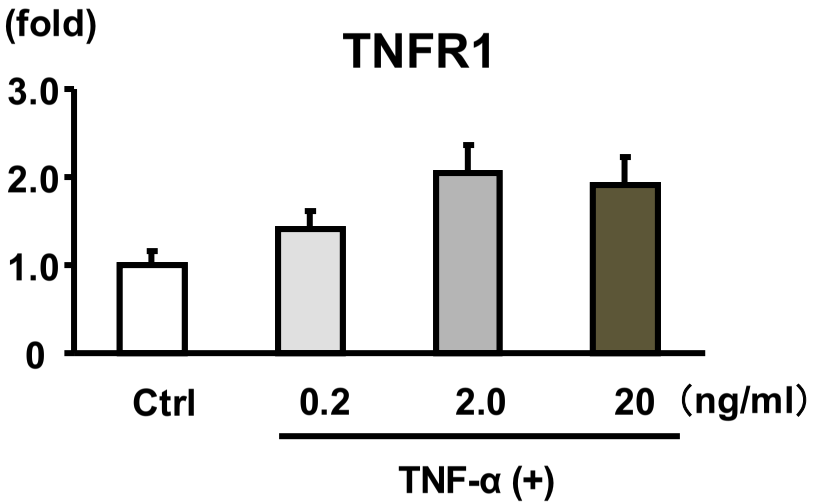

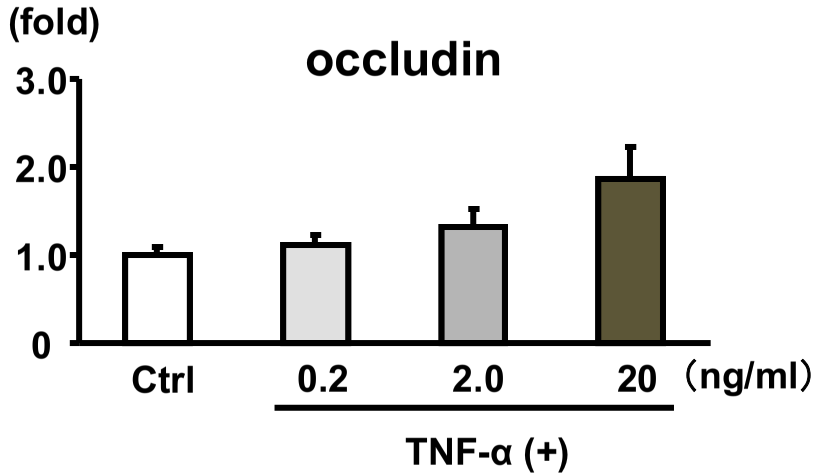

Primers used for quantitative real-time RT-PCR

hTNFR1 Forward	5'-GGTGCTAACCCCTCGATGTA-3'
hTNFR1 Reverse	5'-GCTTGCTATGTGCTTGTCCA-3'
hZO-1 Forward	5'-AAGAGAAAGGTGAAACACTGCTG-3'
hZO-1 Reverse	5'-GTTTGCTCCAACGAGATAATTTG-3'
hOccludin Forward	5'-GAAGCCAAACCTCTGTGAGC-3'
hOccludin Reverse	5'-GAAGACATCGTCTGGGGTGT-3'

Supplementary Figure 7

Quantitative RT-PCR analysis of the expression of ZO-1, occludin, and TNFR1 expression with or without TNF-α treatment

The mRNA expression of ZO-1 was unchanged by the TNF-α treatment. The higher dose of TNF-α showed slight elevations of occludin and TNFR1.

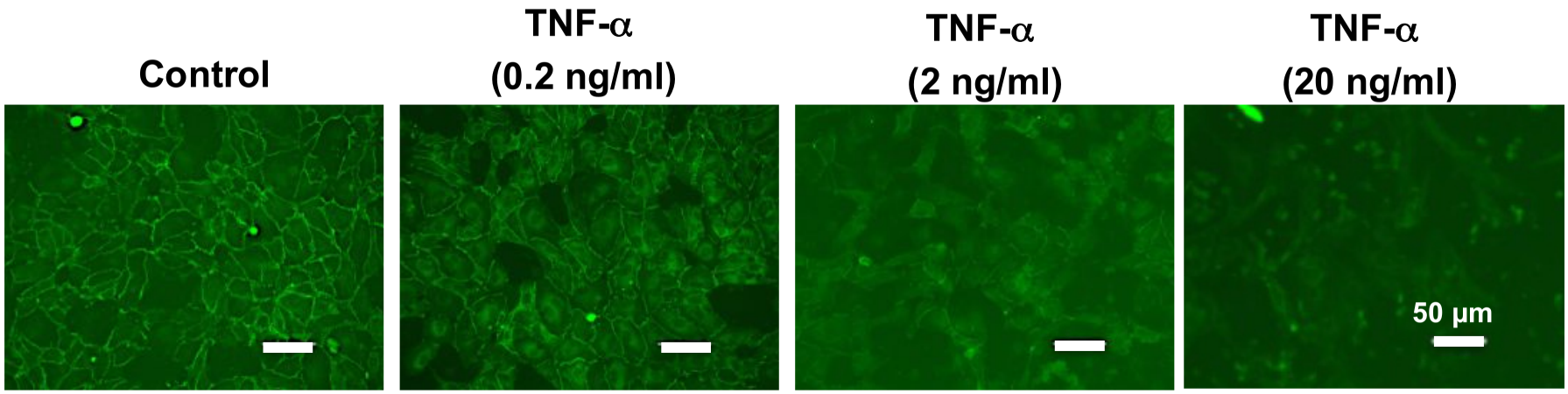

Supplementary Figure 8

Immunostaining of ZO-1-positive tight junctions between cultured vascular endothelial cells
Administration of TNF-α to the endothelial cells (HUVEC) dose-dependently enhanced disruption of ZO-1-positive tight junctions. Bars = 50 μm.

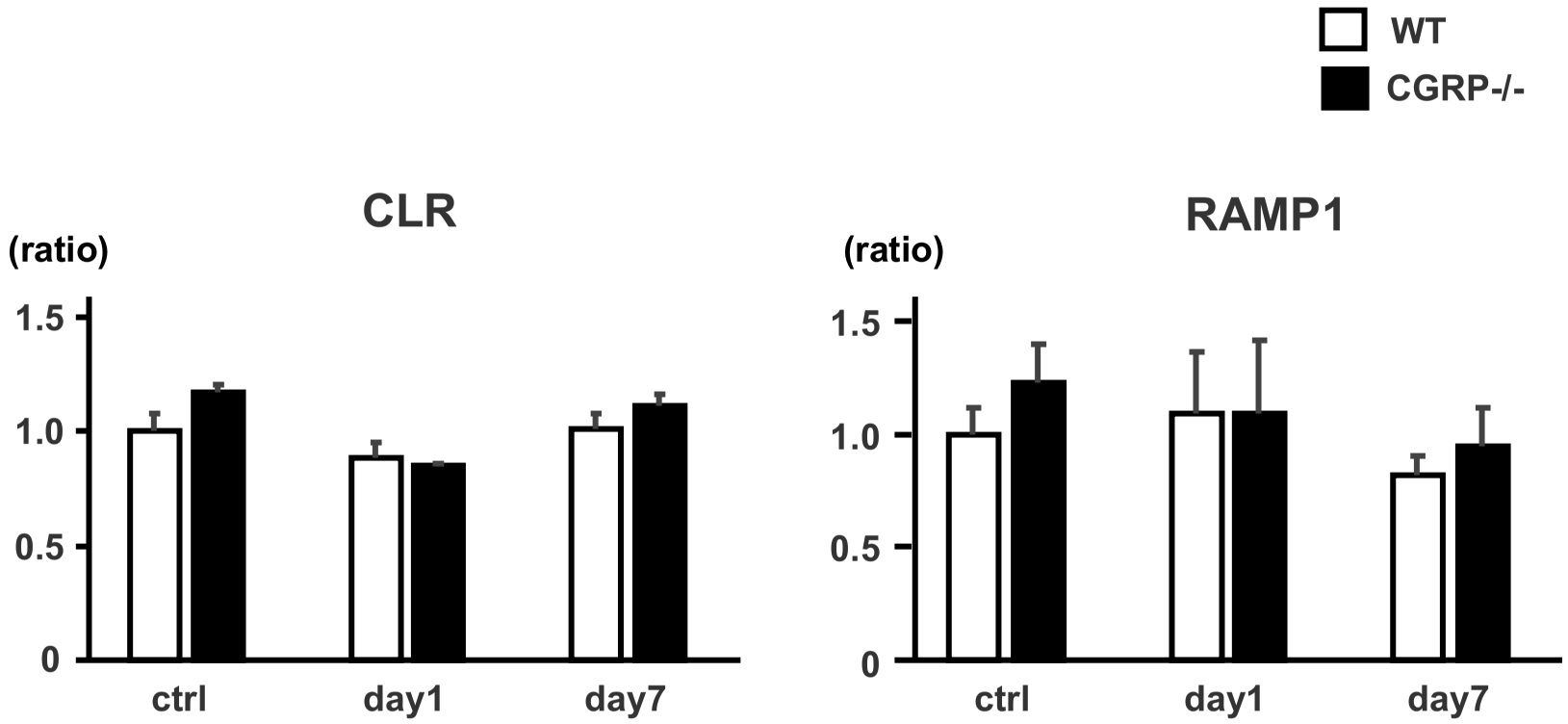

Supplementary Figure 9

Expression of CGRP receptor components during CNV

By quantitative RT-PCR analysis of the choroid, we evaluated the mRNA levels during CNV. Expression of the CGRP receptor components CLR and RAMP1 was not markedly changed during CNV in either WT or CGRP-/- mice. Bars are means ± SEM. n = 4.